Atmospheric Research 216 (2019) 86–105

Contents lists available at ScienceDirect

Atmospheric Research

journal homepage: www.elsevier.com/locate/atmosres

Invited review article

Turbulent Prandtl number in the atmospheric boundary layer - where are we now?

Dan Li*

Department of Earth and Environment, Boston University, Boston, MA 02215, USA

ARTICLE INFO

Keywords:
Atmospheric boundary layer
Cospectral budget model
Thermal stratification
Turbulent Prandtl number

ABSTRACT

First-order turbulence closure schemes continue to be work-horse models for weather and climate simulations. The turbulent Prandtl number, which represents the dissimilarity between turbulent transport of momentum and heat, is a key parameter in such schemes. This paper reviews recent advances in our understanding and modeling of the turbulent Prandtl number in high-Reynolds number and thermally stratified atmospheric boundary layer (ABL) flows. Multiple lines of evidence suggest that there are strong linkages between the mean flow properties such as the turbulent Prandtl number in the atmospheric surface layer (ASL) and the energy spectra in the inertial subrange governed by the Kolmogorov theory. Such linkages are formalized by a recently developed cospectral budget model, which provides a unifying framework for the turbulent Prandtl number in the ASL. The model demonstrates that the stability-dependence of the turbulent Prandtl number can be essentially captured with only two phenomenological constants. The model further explains the stability- and scale-dependences of the subgrid-scale Prandtl number in large-eddy simulation. The connections between mean flow properties and microscale energy distributions shed novel insights into the breakdown of Monin-Obukhov similarity theory under strongly stable conditions.

1. Introduction

The title of this review is inspired by the classic review by Kays published more than twenty years ago titled *"Turbulent Prandtl Number - Where Are We?"* (Kays, 1994). The similarity between the two titles, both in the form of a question, is meant to provoke discussions about advances in our understanding of the turbulent Prandtl number, and more broadly turbulent momentum and heat transfer, over the last two decades. This review nonetheless has a different focus compared to the review by Kays, which primarily addressed the turbulent Prandtl number in engineering flows (Kays, 1994). This review is dedicated to the turbulent Prandtl number in the atmospheric boundary layer (ABL), which is the lowest 1–2 km of the atmosphere directly influenced by the Earth's surface and is the home for most human activities and biological processes (Stull, 1988).

The study of turbulent momentum and heat transfer in the atmosphere has a long history. In fact, the origin of the turbulent Prandtl number concept is rooted in early studies of heat transfer in the atmosphere. In his seminal paper *"Eddy Motion in the Atmosphere"*, Taylor (1915) proposed the concept of 'eddy diffusivity' for describing heat transfer by the turbulent wind field in analogy of 'thermal diffusivity' for describing molecular diffusion of heat. This, along with Boussinesq's 'eddy viscosity' hypothesis in analogy of 'molecular viscosity' (see discussions in Frisch (1995)), forms the basis of so-called first-order turbulence closures to the Reynolds-averaged Navier-Stokes (RANS) equations and gives rise to the turbulent Prandtl number (Pr_t), which is simply the ratio of the eddy viscosity (K_m) to the eddy diffusivity for heat (K_h). Nowadays nearly all atmospheric models for weather and climate simulations are based on RANS equations and many of them are still employing first-order turbulence closures (Stensrud, 2007), where Pr_t can be viewed as a key input linking the eddy diffusivity for heat (K_h) to the eddy viscosity (K_m). Even in large-eddy simulations (LES) that are becoming increasingly popular in atmospheric research, a subgrid-scale Prandtl number (Pr_{SGS}) is needed and is often parameterized, although the role of subgrid-scale Prandtl number (Pr_{SGS}) is less significant than that of turbulent Prandtl number (Pr_t) due to the fact that the large-scale fluxes are resolved in LES.

Strictly speaking the turbulent Prandtl number is a concept pertinent to turbulent heat transfer. However, the significance of turbulent Prandtl number in atmospheric research often goes beyond that. This is because atmospheric models tend to assume that the turbulent wind field transports all scalars such as water vapor, CO_2, CH_4 and NH_3 in a similar way as heat, despite that temperature is an active scalar that can alter the flow field and has a feedback impact on heat flux while the

* Corresponding author.
E-mail address: lidan@bu.edu.

https://doi.org/10.1016/j.atmosres.2018.09.015
Received 7 June 2018; Received in revised form 20 August 2018; Accepted 17 September 2018
Available online 25 September 2018

other scalars are passive scalars that do not alter the flow field. In other words, the turbulent Schmidt number, which is the counterpart of the turbulent Prandtl number for mass transfer (Gualtieri et al., 2017), is often assumed to be identical to the turbulent Prandtl number in atmospheric models. As a result, a better understanding and parameterization of the turbulent Prandtl number in the atmosphere is not only helpful for improving weather and climate predictions and applications related to heat transfer, but also has significant implications for air quality, agricultural management, ecosystem services, to name a few. In particular, the importance of turbulent Prandtl/Schmidt number in atmospheric dispersion modeling with Computational Fluid Dynamics (CFD) tools has been widely recognized (see a recent review by Tominaga and Stathopoulos (2013)).

To start, it is essential to highlight a number of unique features of the ABL flow. First of all, the horizontal scale of the ABL is usually orders of magnitude larger than the vertical scale. In this sense, the ABL resembles a two-dimensional, wall-bounded turbulent boundary layer. This feature of the ABL provides a good justification to the use of first-order turbulence closure schemes in atmospheric models, except in regions where non-local transport becomes important including the mixed layer under strongly unstable conditions, the canopy layer, and the roughness sublayer (see Fig. 1 for a schematic of the ABL structure over a canopy). These regions will be excluded from this review, despite that in practice first-order turbulence closure schemes with some modifications (e.g., adding non-local terms, see Holtslag and Moeng (1991) for an example) continue to be used in these regions. Second, the Reynolds number and turbulent Peclet number of the ABL are typically very large (on the order of 10^8). A direct consequence is that the effects of molecular viscosity and thermal diffusivity are confined within an extremely thin ($\approx$1 mm) layer at the interface between the Earth's surface and the atmosphere (i.e., the viscous sublayer). As a result, the dependence of turbulent Prandtl number on molecular viscosity and thermal diffusivity in the near-wall region, a topic extensively studied in laboratory experiments and with direct numerical simulations (DNS) (Kays, 1994), is typically not a concern for the ABL flow. Lastly, while the Reynolds analogy (i.e., $Pr_t = 1$) or a constant but smaller than unity value of Pr_t continues to find its way in engineering applications, atmospheric scientists discovered the role of thermal stratification in inducing dissimilarity between turbulent transport of momentum and heat as early as 1940s (Ertel, 1942; Priestley and Swinbank, 1947). The significance of thermal stratification in the ABL is now well recognized, especially in the atmospheric surface layer (ASL, see Fig. 1) where Monin-Obukhov Similarity Theory (MOST) provides a theoretical framework for parameterizing turbulent fluxes under the influence of thermal stratification.

With these features of the ABL flow in mind, this paper reviews recent advances in our understanding and parameterization of turbulent Prandtl number in the ABL since 1990s. Before discussing the scope and organization of this review, the definition of the turbulent Prandtl number and the necessary background are provided.

2. The turbulent Prandtl number

In this section, the definition and the significance of turbulent Prandtl number are discussed within the framework of RANS modeling. For the purpose of illustration, a horizontally homogeneous, two-dimensional (x-z) dry ABL that satisfies the Boussinesq approximation is considered. The budget equations for the mean longitudinal velocity and potential temperature are as follows

$$\frac{\partial \overline{u}}{\partial t} + \overline{w}\frac{\partial \overline{u}}{\partial z} = -\frac{1}{\overline{\rho}}\frac{\partial \overline{p}}{\partial x} + \frac{\partial}{\partial z}\left(\nu\frac{\partial \overline{u}}{\partial z} - \overline{u'w'}\right), \tag{1}$$

$$\frac{\partial \overline{\theta}}{\partial t} + \overline{w}\frac{\partial \overline{\theta}}{\partial z} = \frac{\partial}{\partial z}\left(D\frac{\partial \overline{\theta}}{\partial z} - \overline{w'\theta'}\right), \tag{2}$$

where u, w, and θ are the longitudinal velocity, vertical velocity, and potential temperature, respectively; p is the pressure; ρ is the air density; ν and D are the molecular viscosity and thermal diffusivity, respectively. The overbar indicates the Reynolds average and the prime indicates turbulent excursions from the averaged state. Here $\overline{u'w'}$ is the vertical turbulent momentum flux and $\overline{w'\theta'}$ is the vertical turbulent heat flux. Note that the Coriolis force is not included due to the assumption of two-dimensional ABL.

In first-order turbulence closure schemes, turbulent fluxes are related to the *local* gradients of the mean variables:

$$\overline{u'w'} = -K_m\frac{\partial \overline{u}}{\partial z} = -K_m \mathrm{S}, \tag{3}$$

$$\overline{w'\theta'} = -K_h\frac{\partial \overline{\theta}}{\partial z} = -K_m \Gamma, \tag{4}$$

where $\mathrm{S} = \partial\overline{u}/\partial z$ and $\Gamma = \partial\overline{\theta}/\partial z$ are the vertical gradients of mean longitudinal velocity and potential temperature, respectively; K_m and K_h are the eddy viscosity and eddy diffusivity for heat, respectively. The

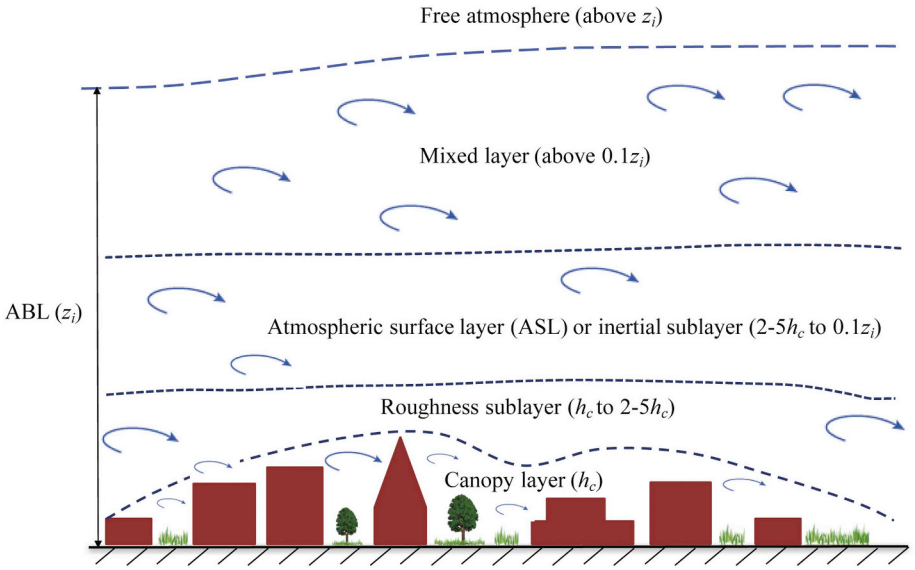

Fig. 1. A schematic of the structure of ABL of height z_i over an urban canopy of averaged height h_c (do not scale). Only unstable conditions with strong turbulent mixing are shown.

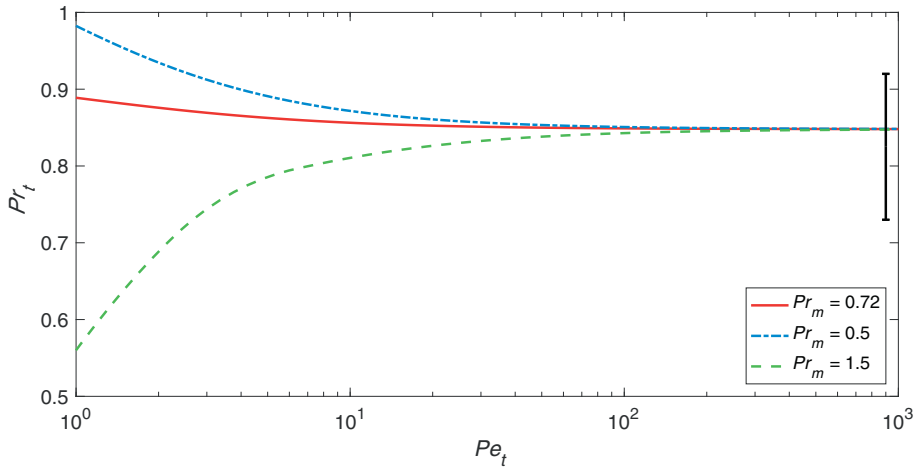

Fig. 2. The relation between turbulent Prandtl number (Pr_t) and turbulent Peclet number (Pe_t) for air flows ($Pr_m = 0.72$, red line) from the RNG method (Yakhot et al., 1987). Also shown are the results with $Pr_m = 0.5$ and $Pr_m = 1.5$. The bar indicates the range of experimentally determined Pr_t in the laboratory for air flows (Kays, 1994).

ratio of K_m to K_h is the turbulent Prandtl number

$$Pr_t = \frac{K_m}{K_h} \tag{5}$$

It is clear that the turbulent Prandtl number is essentially an indication of *dissimilarity* between turbulent transport of momentum and heat. The assumption that heat is transported in a similar way as momentum in turbulent flows, namely $Pr_t = 1$, is called the Reynolds analogy. These first-order turbulence closure schemes are also called flux-gradient relations, eddy-diffusivity models, or simply K-theory in the literature (Stull, 1988). Throughout the article, they will be used interchangeably and they all refer to the relations between turbulent fluxes and *local* gradients.

The turbulent Prandtl number Pr_t is a function of the flow and thus is fundamentally different from its molecular counterpart (hereafter called the molecular Prandtl number Pt_m)

$$Pr_m = \frac{\nu}{D}, \tag{6}$$

which is a function of the fluid (Tennekes and Lumley, 1972). The value of Pr_m is about 0.72 for air mixture under typical atmospheric conditions. In fact most gases (e.g., methane, oxygen, CO_2) under typical atmospheric conditions have Pr_m values on the order of unity (Rohsenow et al., 1998).

Substituting the above equations into Eqs. (1) and (2) and neglecting the molecular effects (i.e., assuming sufficiently high Reynolds and turbulent Peclet numbers) yield

$$\frac{\partial \overline{u}}{\partial t} + \overline{w}\frac{\partial \overline{u}}{\partial z} = -\frac{1}{\overline{\rho}}\frac{\partial \overline{p}}{\partial x} + \frac{\partial}{\partial z}\left[K_m \frac{\partial \overline{u}}{\partial z}\right], \tag{7}$$

$$\frac{\partial \overline{\theta}}{\partial t} + \overline{w}\frac{\partial \overline{\theta}}{\partial z} = \frac{\partial}{\partial z}\left[\frac{K_m}{Pr_t}\frac{\partial \overline{\theta}}{\partial z}\right] \tag{8}$$

It is clear that K_m and Pr_t (or equivalently K_m and K_h) are two critical inputs for predicting the mean flow properties such as $\overline{u}$ and $\overline{\theta}$.

3. Background

3.1. High-Reynolds number, neutrally stratified turbulent boundary layers and the logarithmic region

In classic boundary layer theory, a wall-bounded turbulent boundary layer that does not experience any buoyancy effect (i.e., neutrally stratified) is often described by a two-layer structure: an inner layer and an outer layer (Tennekes and Lumley, 1972). When the Reynolds number is large enough, there exits an overlap or matched layer in which both mean velocity and temperature profiles are logarithmic. In this logarithmic region, the Pr_t should be independent of the distance from the wall and can be inferred from the slopes of the normalized mean velocity and temperature profiles (Kays, 1994). For air flows, the Pr_t determined this way in laboratory experiments ranges from 0.73 to 0.92 (Kays, 1994).

Many analytical and empirical formulations for Pr_t derived from a variety of models exist in the literature as reviewed elsewhere (Reynolds, 1975; Kays, 1994). Here only one notable example, which is the result from the renormalization group (RNG) method (Yakhot et al., 1987), is discussed. The Pr_t from the RNG method is determined using the following formulation:

$$\left[\frac{\frac{1+\frac{Pe_t}{Pr_t}}{\frac{Pr_m+Pe_t}{Pr_m}} - 1.1793}{\frac{1}{Pr_m} - 1.1793}\right]^{0.65}\left[\frac{\frac{1+\frac{Pe_t}{Pr_t}}{\frac{Pr_m+Pe_t}{Pr_m}} + 2.1793}{\frac{1}{Pr_m} + 2.1793}\right]^{0.35} = \frac{1}{1+\frac{Pe_t}{Pr_m}}, \tag{9}$$

where

$$Pe_t = (K_m/\nu)Pr_m \tag{10}$$

is the turbulent Peclet number indicating the relative importance of advective transport and diffusive transport (Kays, 1994). Note that (K_m/ν) can be interpreted as the Reynolds number and hence a high Reynolds number always indicates a high turbulent Peclet number for air flows with $Pr_m = 0.72$. The reason that Pe_t defined based on K_m is used is because Pr_t is also related to K_m so that Pr_t could be linked to Pe_t once Pr_m is known.

It is clear from Eq. (9) that if Pr_m was known (i.e., for a given fluid), the RNG method would provide a relation between Pr_t and Pe_t, as shown in Fig. 2, which presents the relations between Pr_t and Pe_t for air flows (red line, $Pr_m = 0.72$) and two other fluids with $Pr_m = 0.5$ and $Pr_m = 1.5$ in order to cover a range of gases of interest to atmospheric scientists. It can be seen that at sufficiently large values of Pe_t (e.g., in the ABL), the Pr_t approaches a value of about 0.85 (Yakhot et al., 1987), which is within the range of laboratory results (Kays, 1994). More importantly, the asymptotic behavior of Pr_t at large values of Pe_t is independent of the value of Pr_m (at least for the range of Pr_m considered here), suggesting that the turbulent Prandtl number in the ABL is hardly controlled by its molecular counterpart.

The exact value of Pr_t in the logarithmic region of high-Reynolds number, neutrally stratified turbulent boundary layers (and also other wall-bounded turbulent flows such as pipe and channel flows) continues to be debated. With fast growing computational resources, DNS may be a promising tool to address this question (Kasagi et al., 1992; Kawamura et al., 1998, 1999; Kong et al., 2000; Abe et al., 2004; Redjem-Saad et al., 2007) as it does not require any turbulence model. However, the Reynolds numbers of current DNS studies are fairly low

(Kajishima and Taira, 2017) and fully resolving this issue awaits further increases in computational resources to allow DNS of high-Reynolds number turbulent flows.

3.2. Monin-Obukhov Similarity Theory (MOST)

In the ABL, the logarithmic region is often called the inertial sublayer or the atmospheric surface layer (ASL), which roughly corresponds to the lowest 10% of the ABL that is also above the canopy layer and roughness sublayer (see Fig. 1). The ASL is probably the most extensively studied part of the ABL both experimentally over short canopies ($h_c \ll 0.1z_i$) and theoretically. Compared to the classic boundary layers studied in the laboratory, the ASL is constantly affected by the presence of thermal stratification or buoyancy resulting from surface heating and cooling in a diurnal cycle. As a result of the buoyancy effect, the logarithmic profiles are modified and the turbulent Prandtl number varies strongly with atmospheric stability.

Using only dimensional considerations, Monin and Obukhov (1954) showed that distortions to the classical logarithmic profiles by buoyancy can be accounted for by stability correction functions that are only functions of the so-called stability parameter (ζ) (Obukhov, 1946; Monin and Obukhov, 1954; Businger and Yaglom, 1971). For mean horizontal velocity and potential temperature, the stability correction functions are denoted as ϕ_m and ϕ_h, respectively, given as:

$$\phi_m(\zeta) = \frac{\kappa z}{u_*}\mathrm{S}, \tag{11}$$

$$\phi_h(\zeta) = \frac{\kappa z}{\theta_*}\Gamma, \tag{12}$$

where $\kappa \approx 0.4$ is the von Kármán constant, z is height from the ground surface or zero-plane displacement, $u_* = (-\overline{u'w'})^{1/2}$ is the friction velocity, and $\theta_* = -\overline{w'\theta'}/u_*$ is a temperature scaling parameter. The stability parameter $\zeta = z/L$ where $L = -u_*^3/(\kappa\beta\overline{w'\theta'})$ is the Obukhov length (Obukhov, 1946), $\beta = g/\overline{\theta}$ is the buoyancy parameter, g is the gravitational acceleration rate.

When $\zeta < 0$, which corresponds to $\overline{w'\theta'} > 0$, the ASL is unstable (e.g, during daytime) and when $\zeta > 0$, which corresponds to $\overline{w'\theta'} < 0$, the ASL is stable (e.g, during nighttime). When $\zeta = 0$, the ASL is labeled as neutrally buoyant (or neutral). Based on these definitions, the Pr_t can be related to the stability correction functions following

$$Pr_t = \frac{\phi_h(\zeta)}{\phi_m(\zeta)} \tag{13}$$

Evidently, Pr_t is also only a function of the stability parameter (ζ) in the MOST framework.

It is important to point out that MOST assumes that the ASL flow is stationary, planar homogeneous and without subsidence, characterized by sufficiently high Reynolds and turbulent Peclet numbers, and lacks any strong horizontal pressure gradients. When these assumptions are applied to the mean momentum (Eq. (1)) and mean potential temperature (Eq. (2)) budgets, the outcome is that the turbulent momentum and heat fluxes ($\overline{u'w'}$ and $\overline{w'\theta'}$) become independent of z. It is for this reason that the ASL is often labeled as the 'constant-flux layer'. In the following, the ASL that satisfies all the MOST assumptions will be called an idealized ASL.

Another important indicator of atmospheric stability effect is the Richardson number. In fact, there are two widely used Richardson numbers: the gradient Richardson number (R_g) and the flux Richardson number (R_f), defined as,

$$R_g = \frac{\beta\Gamma}{\mathrm{S}^2}, \tag{14}$$

and

$$R_f = -\frac{\beta\overline{w'T'}}{-\mathrm{S}\overline{u'w'}}, \tag{15}$$

respectively. With these two Richardson numbers, it can be shown that

$$Pr_t = \frac{R_g}{R_f} \tag{16}$$

3.3. The role of buoyancy in heat transport

Before presenting the experimentally determined ϕ_m and ϕ_h in the ASL, it is enlightening to examine how buoyancy introduces dissimilarity in turbulent transport of momentum and heat from the perspective of momentum and heat flux budgets. The role of buoyancy in heat transport was recognized as early as 1940s by Ertel (1942) and Priestley and Swinbank (1947). However, instead of presenting the original arguments in Ertel (1942) and Priestley and Swinbank (1947), a derivation based on the modern understanding of turbulent transport in the ASL (Li et al., 2012b) is shown here to illustrate how buoyancy enhances (suppresses) turbulent transport of heat under unstable (stable) conditions.

With the same assumptions of MOST, the budget equations for turbulent momentum and heat fluxes can be simplified into

$$\frac{\partial\overline{u'w'}}{\partial t} = 0 = -\overline{w'w'}\mathrm{S} - \frac{\partial\overline{w'w'u'}}{\partial z} - \frac{1}{\rho}\overline{u'\frac{\partial p'}{\partial z}} + \beta\overline{u'T'} - 2\nu\overline{\frac{\partial u'}{\partial z}\frac{\partial w'}{\partial z}}, \tag{17}$$

$$\frac{\partial\overline{w'\theta'}}{\partial t} = 0 = -\overline{w'w'}\Gamma - \frac{\partial\overline{w'w'\theta'}}{\partial z} - \frac{1}{\rho}\overline{\theta'\frac{\partial p'}{\partial z}} + \beta\overline{\theta'\theta'} - (\nu + D_m)\overline{\frac{\partial w'}{\partial z}\frac{\partial\theta'}{\partial z}} \tag{18}$$

The terms on the right hand-side of the equations represent (in order): production terms due to the presence of mean velocity and potential temperature gradients, flux-transport terms that represent turbulent transport of momentum and heat fluxes, pressure-decorrelation terms due to interactions between pressure and velocity and pressure and temperature, buoyancy terms arising from thermal stratification, and molecular destruction terms. The molecular destruction terms are usually much smaller than the pressure-decorrelation terms and are often also neglected (Wyngaard, 2010). In addition, the turbulent transport terms and the correlation between u and T are typically small in an idealized ASL (Katul et al., 2014). With these additional assumptions, the above budgets are further simplified into

$$0 = -\overline{w'w'}\mathrm{S} - \frac{1}{\rho}\overline{u'\frac{\partial p'}{\partial z}}, \tag{19}$$

$$0 = -\overline{w'w'}\Gamma - \frac{1}{\rho}\overline{\theta'\frac{\partial p'}{\partial z}} + \beta\overline{\theta'\theta'} \tag{20}$$

The Rotta model (Rotta, 1951) is further invoked for parametrizing the pressure-decorrelation terms (Mellor and Yamada, 1974; Yamada, 1975; Mellor and Yamada, 1982; Moeng and Wyngaard, 1986; Pope, 2000). For illustration only the linear (or slow) component is retained, as follows:

$$-\frac{1}{\rho}\overline{u'\frac{\partial p'}{\partial z}} = -C_u\frac{\overline{u'w'}}{\tau_u}, \tag{21}$$

$$-\frac{1}{\rho}\overline{\theta'\frac{\partial p'}{\partial z}} = -C_\theta\frac{\overline{w'\theta'}}{\tau_\theta}, \tag{22}$$

where τ is the relaxation time scale that indicates how fast a turbulent eddy dissipates its energy or loses its coherency and C is a coefficient. Substituting the linear Rotta model into Eqs. (19) and (20) produces

$$\overline{u'w'} = \frac{\tau_u}{C_u}(-\overline{w'w'}\mathrm{S}), \tag{23}$$

$$\overline{w'\theta'} = \frac{\tau_\theta}{C_\theta}(-\overline{w'w'}\Gamma + \beta\overline{\theta'\theta'}) \tag{24}$$

Eq. (24) recovers the results of Ertel (1942) and Priestley and

Swinbank (1947) where the additional buoyancy term was first recognized. It clearly shows how the so-called 'convective turbulence' (related to $\overline{\theta'\theta'}$) modulates turbulent heat flux in a different way than 'mechanical turbulence' (related to $\overline{w'w'}$).

Pr_t can be readily determined from Eqs. (23) and (24):

$$Pr_t = \frac{\tau_u C_\theta}{\tau_\theta C_u}\left(\frac{1}{1-\frac{\beta}{\Gamma}\frac{\overline{\theta'\theta'}}{\overline{w'w'}}}\right) \tag{25}$$

Under neutral conditions, $Pr_{t,\ neu} = (\tau_u C_\theta)/(\tau_\theta C_u)$, where the subscript 'neu' indicates 'neutral conditions'. Clearly, under unstable conditions ($\Gamma < 0$), $Pr_t < Pr_{t,\ neu}$ and under stable conditions ($\Gamma > 0$), $Pr_t > Pr_{t,\ neu}$. This suggests that compared to turbulent transport of momentum, turbulent transport of heat is enhanced (suppressed) under unstable (stable) conditions. Further relating Pr_t to atmospheric stability indicators such as ζ and Richardson numbers requires considerations of the governing equations for $\overline{w'w'}$ and $\overline{\theta'\theta'}$ (for example in second-order turbulence closure models), which will be discussed later.

It is important to stress that in this derivation the dissimilarity between turbulent transport of momentum and heat stems solely from the buoyancy effect, while the non-stationary, advection, and third-order flux-transport terms in the momentum and heat flux budgets have been neglected. In the real atmosphere, these terms may also play a role in inducing dissimilarity between turbulent transport of momentum and heat.

3.4. The Businger-Dyer relations

The functional forms of ϕ_m and ϕ_h have been the subject of field experimental research in the 1960–1980s when the eddy covariance technique started to become mature, enabling a direction quantification of turbulent fluxes (Stull, 1988). The field experiments conducted in this period, most notably the Kansas experiment in 1968, have shaped our understanding of ϕ_m and ϕ_h and thus Pr_t in the ASL to date. From these field experiments dozens of functional forms for ϕ_m and ϕ_h have been proposed. Fig. 3 shows the Pr_t determined from fitted functions for ϕ_m and ϕ_h in two most influential studies during this period (Businger et al., 1971; Dyer, 1974). Nowadays these functions are commonly called the 'Businger-Dyer relations' (Businger, 1988). The functional forms for Pr_t from Businger et al. (1971) and Dyer (1974) are

$$Pr_t = \frac{\phi_h}{\phi_m} = \begin{cases} \frac{0.74(1-9\zeta)^{-\frac{1}{2}}}{(1-15\zeta)^{-\frac{1}{4}}}, & \zeta < 0 \\ \frac{0.74+4.7\zeta}{1+4.7\zeta}, & \zeta > 0 \end{cases},$$

$$Pr_t = \frac{\phi_h}{\phi_m} = \begin{cases} \frac{(1-16\zeta)^{-\frac{1}{2}}}{(1-16\zeta)^{-\frac{1}{4}}}, & \zeta < 0 \\ 1, & \zeta > 0 \end{cases},$$

respectively.

It can be seen from Fig. 3 that both functions suggest that the Pr_t decreases as the atmosphere becomes more unstable. The major difference between the two functions is the Pr_t under neutral conditions ($Pr_{t,\ neu}$), which is 0.74 in the Businger relation but 1 in the Dyer relation, and the behavior of Pr_t under stable conditions. A review by Högström (1988), which compared the Businger-Dyer relations to a few other experimental studies and used $\kappa = 0.4$ consistently across data sets, confirmed that the decrease of Pr_t under unstable conditions is very robust, while under neutral and stable conditions the scatter of data is too large to determine whether Pr_t is significantly different from unity and whether Pr_t continues to increase with increasing ζ. These findings are anchored by other review articles (Högström, 1996; Andreas, 2002; Foken, 2006) and more recent experiments (Song et al., 2010; Liu et al., 2016). One caveat of Fig. 3 is that the Businger-Dyer relations, and many other empirical formulations, were proposed based on data collected primarily in the range of $-2 < \zeta < 2$ but here the results in the range of $-10 < \zeta < 10$ are shown for illustration purposes.

4. Scope and organization

By the time Kays' review was published, it was already known, both theoretically and experimentally, that turbulent transport of heat in the ABL relative to turbulent transport of momentum is enhanced under unstable conditions due to the role of buoyancy. However, the behavior of Pr_t in stable ABLs remains elusive. From the extensive laboratory and field experiments and theoretical work such as the RNG method one expects the neutral value of Pr_t to range from 0.7 to 0.9 or so in the ABL. All of these form the starting point of this review.

In the following, new developments in our understanding and modeling of Pr_t in the ABL since 1990s are reviewed, with a focus on presenting a unifying framework for Pr_t in the ASL based on a recently developed cospectral budget model. Sections 5 and Section 6 examine the Pr_t in unstable and stable conditions, respectively. The cospectral budget model that provides a unifying framework for Pr_t in the ASL is then reviewed in Section 7. Further application of the cospectral budget model to studying the subgrid-scale Prandtl number (Pr_{SGS}) is discussed in Section 8. Conclusions are presented in Section 9, which also discusses future research priories.

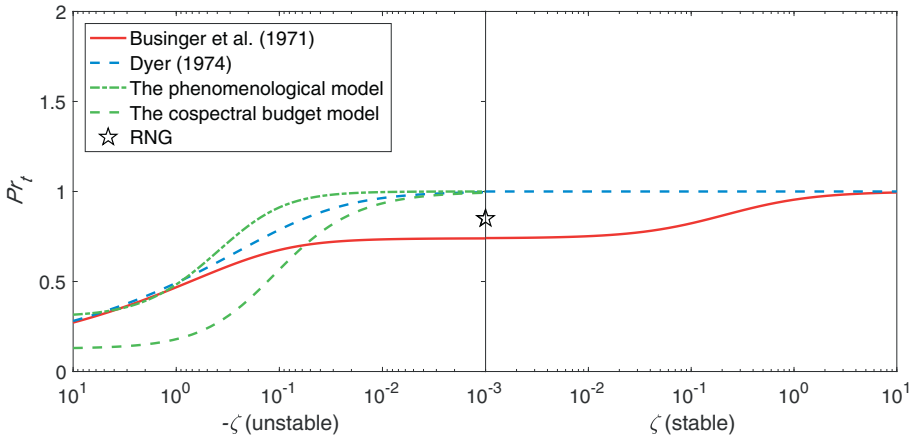

Fig. 3. The Pr_t from 'Businger-Dyer' relations for ϕ_m and ϕ_h determined by field experiments. The phenomenological model (Li et al., 2012b) and the cospectral budget model (Li et al., 2015b) results are also shown for unstable conditions. The neutral value of Pr_t from the RNG method (Yakhot et al., 1987) is shown as a reference.

5. Pr_t and coherent structures in unstable ABLs

As discussed earlier, nearly all field data and simplifications of the flux budgets suggest that Pr_t decreases as the atmosphere becomes more unstable (see Fig. 3). New understanding of this well-established result is generated by recent advances in our knowledge of coherent structures or organized motions in turbulent flows, which are broadly defined as flow features that persist in space and time. Reviews of coherent structures in high-Reynolds number turbulent flows can be found elsewhere (Cantwell, 1981; Robinson, 1991; Adrian, 2007; Marusic et al., 2010; Smits et al., 2011). Here only a general picture is presented to pave the way for discussing the linkage between the phenomenology of turbulence and the dissimilarity between turbulent transport of momentum and heat or Pr_t.

5.1. The impact of atmospheric instability on coherent structures in the ABL

Coherent structures or organized motions in turbulent flows have been the subject of active research over the past few decades (Cantwell, 1981; Robinson, 1991; Adrian, 2007; Marusic et al., 2010; Smits et al., 2011). Various forms of coherent structures such as hairpin vortices, large-scale and very large-scale motions have been discovered and extensively studied in pipe flows, channel flows and turbulent boundary layers in laboratory settings. In the neutral ABL, studies also found turbulent structures similar to those in the laboratory (see Hutchins et al. (2012) for detailed discussions and comparisons, including the nomenclature). In addition, recent review articles have indicated that turbulence and the pressure field in the neutral ABL scale similarly as canonical wall-bounded turbulent flows (Marusic et al., 2010), further suggesting that coherent structures responsible for the scaling are similar.

Under unstable conditions, it is expected that coherent structures are strongly modified by the atmospheric instability. For example, in the limit of free convection, the ABL is expected to resemble Rayleigh-Bénard convection rather than wall-bounded turbulence (Wyngaard, 1985), as suggested by classic LES results (Schmidt and Schumann, 1989). In such a regime, the dominant coherent structures are expected to be rising plumes and thermals (Stull, 1988), whose fingerprints can be detected from the ramp structures in the measured time series of scalar quantities such as temperature (Antonia et al., 1979; Brunet et al., 1992; Zhang et al., 2011).

In studying the transition from a neutral to an unstable ABL, Hommema and Adrian (2003), using smoke visualizations, found evidence of hairpin packets under neutral conditions with inclination angles similar to those observed in laboratory studies. They also observed that under moderately unstable conditions the individual hairpins lifted off the surface, leading to an increase in the inclination angle, which was later confirmed by other field studies (Carper and Porté-Agel, 2004; Chauhan et al., 2013; Liu et al., 2017). Under highly unstable conditions, Hommema and Adrian (2003) could not detect any hairpins but their visualizations clearly depict upward-moving plumes. Using eddy-variance data collected over a uniform lake surface, Li and Bou-Zeid (2011) found that the cross-stream vorticity decreases with increasing instability (see Fig. 4a). They conjectured that as the instability increases turbulent structures transition from roll-type structures, including hairpin vortices attached to the surface that have strong cross-stream vorticity, to cellular-type structures (e.g., plumes and thermals) rotating mainly in the vertical direction. This hypothesis is corroborated by LES runs that span a wide range of instabilities (Shah and Bou-Zeid, 2014a; Patton et al., 2016; Salesky et al., 2017).

While these studies presented ample evidence of coherent structures in the ABL and how their topology changes with increasing instability, they did not provide a direct linkage between changes in coherent structures and the turbulent Prandtl number. The following subsection discusses the implications of modifications on coherent structures by the atmospheric instability for the dissimilarity between turbulent transport of momentum and heat with a phenomenological model.

5.2. A phenomenological model for Pr_t

To connect early ideas of Ertel (1942) and Priestley and Swinbank (1947) with recent evidence of instability-induced changes in coherent structures, Li et al. (2012b) employed a phenomenological model originally developed for studying turbulent transport of momentum under neutral (Gioia et al., 2010) and thermally stratified (Katul et al., 2011) conditions. In the original phenomenological model depicted in Fig. 5(a), turbulent momentum flux is assumed to be generated by the turnover of an isotropic eddy of radius s acting on the mean velocity profile. The isotropic eddy transfers momentum down at a rate $\rho\overline{u}(z+s)v(s)$ and up at a rate $\rho\overline{u}(z-s)v(s)$, resulting in a momentum flux

$$\overline{u'w'} = -a_m v(s)[\overline{u}(z+s) - \overline{u}(z-s)] \approx -a_m v(s)\frac{\partial \overline{u}}{\partial z}2s, \tag{26}$$

where $v(s)$ is the turnover velocity of the isotropic eddy of size s; $\overline{u}(z+s) - \overline{u}(z-s)$ is the net momentum, per unit mass per unit velocity of the turnover eddy, exchanged between $z+s$ and $z-s$; a_m is a proportionality constant.

Following this idea, Li et al. (2012b) assumed that the isotropic eddy similarly transfers heat down at a rate $\rho\overline{\theta}(z+s)v(s)$ and up at a rate $\rho\overline{\theta}(z-s)v(s)$ when the surface sensible heat flux H_s is positive (upward). As such, the turbulent sensible heat flux can be expressed as

$$\overline{w'\theta'} = -a_\theta v(s)[\overline{\theta}(z+s) - \overline{\theta}(z-s)] \approx -a_\theta v(s)\frac{\partial \overline{\theta}}{\partial z}2s \tag{27}$$

Similarly, $\overline{\theta}(z+s) - \overline{\theta}(z-s)$ is the net heat flux, per unit mass per unit velocity of the turnover eddy, exchanged between $z+s$ and $z-s$, and a_θ is also a proportionality constant but can be different from a_m.

Similar to Gioia et al. (2010) and Katul et al. (2011), a logical starting point is to assume that eddies contributing most efficiently to momentum and heat transport are those attached to the surface inspired by Townsend's attached eddy hypothesis (Townsend, 1976). Consequently, $s = z$ and Eqs. (26) and (27) reduce to:

$$2\frac{a_m}{\kappa}\frac{v(z)}{u_*}\phi_m = 1, \tag{28}$$

$$2\frac{a_\theta}{\kappa}\frac{v(z)}{u_*}\phi_h = 1, \tag{29}$$

which immediately leads to

$$Pr_t = \frac{a_m}{a_\theta} \tag{30}$$

even without a priori knowledge of $v(z)$. That is, Pr_t is independent of atmospheric stability. When $a_m = a_\theta$, $Pr_t = 1$. It is thus clear that a simple extension of the original model by Gioia et al. (2010) and Katul et al. (2011) results in the well-known Reynolds analogy under all atmospheric stability conditions (at least a stability-independent Pr_t). This is inconsistent with field experiment data under unstable conditions, which show that Pr_t decreases as instability increases (see Fig. 3).

Within the confines of the phenomenological model, Li et al. (2012b) proposed that across the turnover eddy, the spatial excursions embedded in 'instantaneous' temperature profiles could interact with the turnover velocity thereby creating additional dispersive fluxes, contrary to the Eq. (27) postulating that a turnover eddy is passively acting on the 'averaged' temperature profile that is smooth (see Fig. 5(b1 and b2) for a schematic). This hypothesis of interactions between the vertical velocity and temperature fields was supported by observational evidence that the integral length scale of temperature approaches that of vertical velocity as the instability increases, while the integral length scale of horizontal velocity is always at least an order of magnitude larger than that of vertical velocity (see Fig. 4b).

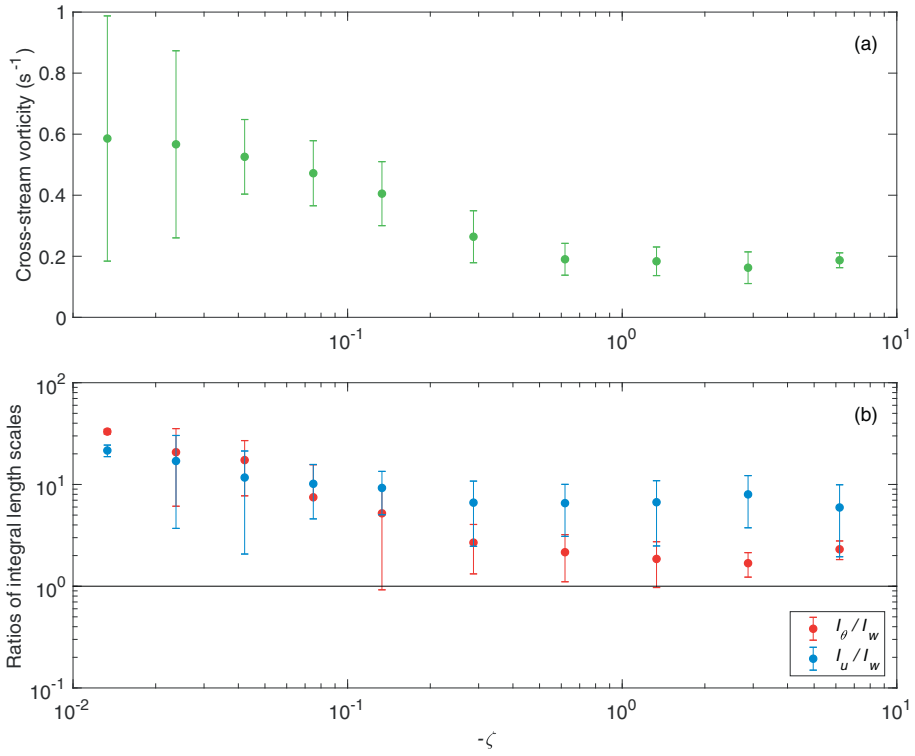

Fig. 4. (a) The standard deviation of cross-stream or spanwise vorticity (s^{-1}) and (b) the ratios of integral length scales (I, where the subscripts θ, u, w represent potential temperature, horizontal velocity, and vertical velocity, respectively) as a function of $-\zeta$ under unstable conditions. The observational data are collected over a lake surface (Vercauteren et al., 2008; Li and Bou-Zeid, 2011; Li et al., 2012a). This figure is based on results in Li and Bou-Zeid (2011) and Li et al. (2012a).

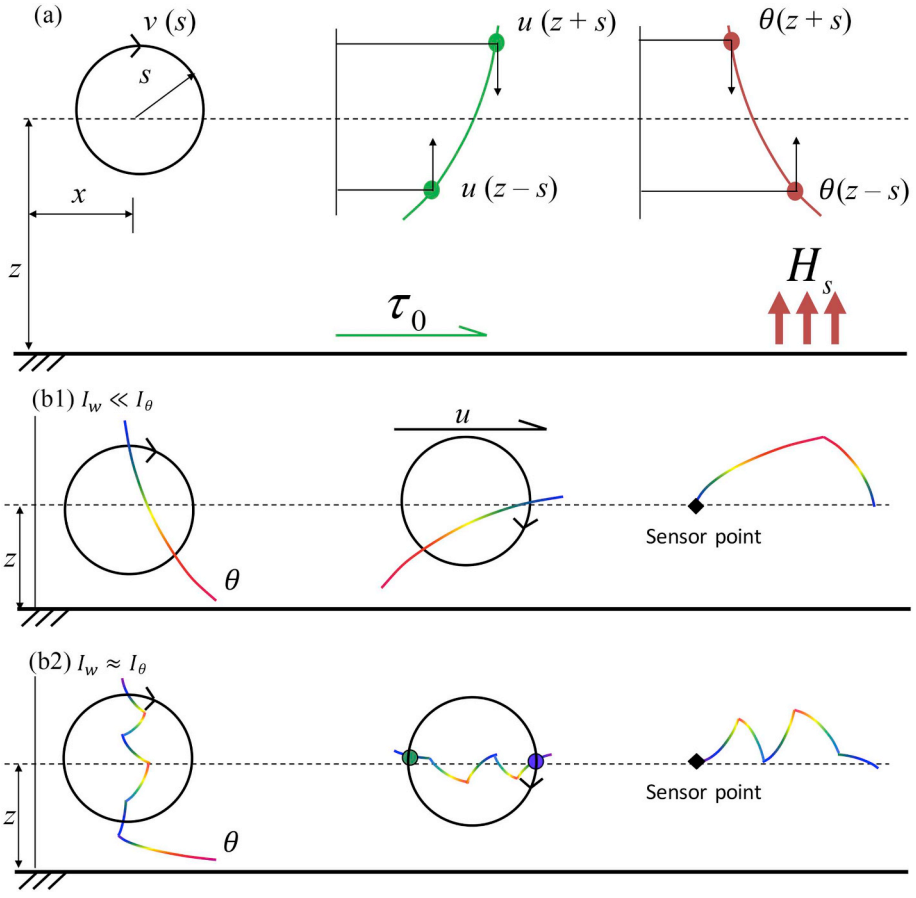

Fig. 5. (a) The phenomenological model for turbulent transport of momentum and heat in the ASL, where τ_o is the surface shear stress and H_s is the surface heat flux. (b1 and b2) Two different cases with different ratios of integral length scales of vertical velocity (I_w) and potential temperature (I_θ). In case (b1), there is no scale-resonance between the vertical velocity and temperature fields. In case (b2), the spatial excursions in the temperature profiles interact with the turnover eddy and create extra heat fluxes (i.e., the scale-resonance effect). The advection and turning of the eddy through a sensor allows one to separate these two cases using integral length scales computed from single-point time series measurements. The figure is adapted from Li et al. (2012b).

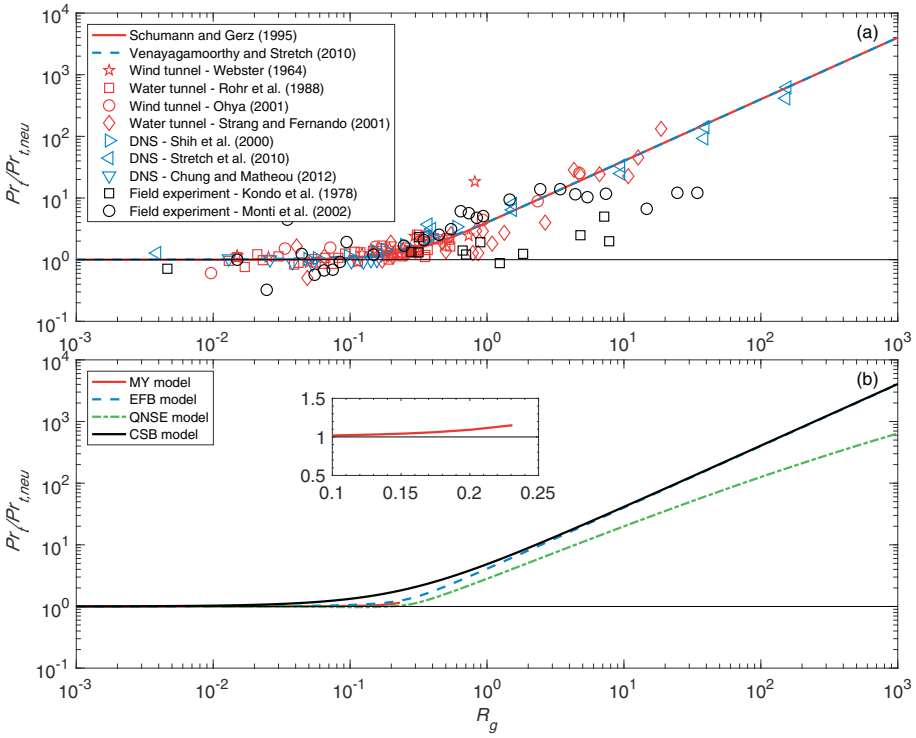

Fig. 6. (a) The Pr_t determined from laboratory experiments (Webster, 1964; Rohr et al., 1988; Ohya, 2001; Strang and Fernando, 2001), numerical simulations (Shih et al., 2000; Stretch et al., 2010; Chung and Matheou, 2012), and field experiments (Kondo et al., 1978; Monti et al., 2002) under stable conditions. The two empirical functions based on merging the asymptotical behaviors of Pr_t are also shown (Schumann and Gerz, 1995; Venayagamoorthy and Stretch, 2010). (b) The Pr_t from the Mellor-Yamada (MY) model, the Energy- and Flux-Budget (EFB) model, the Quasi-Normal Scale Elimination (QNSE) model, and the cospectral budget (CSB) model. The inset shows a closer look at the MY model result, which is limited by the 'critical gradient Richardson number' (R_{gc}).

To account for this 'scale-resonance' between the temperature and vertical velocity fields, a 'resonance' function ($f_\theta(\zeta)$) is included in the phenomenological model, as follows:

$$\overline{w'\theta'} = -a_\theta v(s)[\bar{\theta}(z+s) - \bar{\theta}(z-s)] \approx -a_\theta v(s)\frac{\partial\bar{\theta}}{\partial z}2sf_\theta(\zeta), \tag{31}$$

which leads to

$$2\frac{a_\theta}{\kappa}\frac{v(z)}{u_*}\phi_h = \frac{1}{f_\theta} \tag{32}$$

when $s = z$.

To obtain ϕ_m and ϕ_h explicitly from the model, the turnover eddy velocity $v(z)$ needs to be specified, which is one of the most important assumptions of this phenomenological model and has inspired many future studies (as shall be seen in Section 7). The turnover eddy velocity is assumed to follow the Kolmogorov inertial subrange '1/3' scaling, i.e., $v(z) = [k_\epsilon \epsilon z f_w(\zeta)]^{1/3}$, where k_ϵ is a parameter, ϵ is the mean turbulent kinetic energy (TKE) dissipation rate, and $f_w(\zeta)$ accounts for the anisotropy of the turnover eddy induced by atmospheric instability. The mean TKE dissipation rate (ϵ) can be further estimated by assuming that the TKE budget is in local equilibrium, namely, the shear production and the buoyant production/destruction balances the dissipation rate. With these additional assumptions and the constraints that $\phi_m(0) = 1$, $f_w(0) = 1$, $\phi_h(0) = 1$, $f_\theta(0) = 1$, one arrives at the famous O'KEYPS equation (named after Obukhov, Kazansky, Ellison, Yamamoto, Panofsky, and Sellers, see Lumley and Panofsky (1964)) for both ϕ_m and ϕ_h:

$$\phi_m^4\left(1 - \frac{\zeta}{\phi_m}\right) = \frac{1}{f_w}, \tag{33}$$

$$\phi_h^3\phi_m\left(1 - \frac{\zeta}{\phi_m}\right) = \frac{1}{f_w f_\theta^3} \tag{34}$$

When the functions of f_w and f_θ are determined from experimental data based on how the integral length scales of vertical velocity and temperature vary with instability (see Fig. 4b), the resulting ϕ_m and ϕ_h from this phenomenological model recover their well-established scaling laws as shown in Li et al. (2012b). The Pr_t from this phenomenological model is shown in Fig. 3 and is in fair agreement with the Pr_t in the Businger-Dyer relations under unstable conditions.

Even without the knowledge of $v(z)$, one can obtain the turbulent Prandtl number from the revised phenomenological model as

$$Pr_t = \frac{1}{f_\theta} \tag{35}$$

Thus it is clear that the turbulent Prandtl number is solely determined by the function used to account for the 'scale-resonance' effect and is independent of f_w that indicates the effect of atmospheric instability on the anisotropy of turbulent eddies. This implies that while f_w is critical for correctly capturing the behavior ϕ_m across stability conditions (Katul et al., 2011; Salesky et al., 2013; Li et al., 2016b), the function f_w does not introduce any dissimilarity between turbulent transport of momentum and heat. This further suggests the crucial importance of the 'scale-resonance' effect in inducing dissimilarity between turbulent transport of momentum and heat.

6. Pr_t in stably stratified ABLs

While the behavior of Pr_t under unstable conditions is relatively well understood after the Kansas experiment, its stable counterpart remains elusive. To date, there is still an ongoing debate regarding the behavior of Pr_t under stable conditions (Grachev et al., 2007; Anderson, 2009; Sorbjan and Grachev, 2010; Rodrigo and Anderson, 2013). Although buoyancy is expected to suppresses the transport of heat under stable conditions (see Section 3.3) and in the real atmosphere the existence of gravity waves would further enhance the transport of momentum (Monin and Yaglom, 1971; Mahrt, 1998), experimental evidence is inconclusive especially when Pr_t is presented as a function of ζ. For example, Howell and Sun (1999) found that Pr_t is scattered around unity for ζ up to 10 (similar to the Dyer relation shown in Fig. 3). Andreas (2002) reviewed seven different formulations for ϕ_m and ϕ_h under stable conditions, five of which predict that $Pr_t \to 1$ as $\zeta \to \infty$. Only two predict that Pr_t is not bounded by unity and continues to increase with ζ

even as $\zeta \to \infty$.

On the other hand, when Pr_t is plotted against the gradient Richardson number (R_g), data from field and laboratory experiments and numerical simulations seem to unanimously show that Pr_t increases with R_g (Monin and Yaglom, 1971; Turner, 1979; Bange and Roth, 1999; Zilitinkevich and Calanca, 2000; Zilitinkevich et al., 2008; Kurbatskii and Kurbatskaya, 2010; Vasil'ev et al., 2011; Kitamura et al., 2013; Zilitinkevich et al., 2013; Kurbatskiy and Kurbatskaya, 2014; Aliabadi et al., 2016). A collection of laboratory data from water and wind tunnels, field experimental data, as well as DNS results, is shown in Fig. 6(a). As can be seen, the agreement among these widely different studies is quite remarkable, despite of some scatter associated with the two field experiments. The increase of Pr_t with R_g is also consistent with the theoretical considerations from Section 3.3 as well as the expected role of gravity waves.

Grachev et al. (2007) argued that using experimental data to investigate the behavior of Pr_t under stable conditions is complicated by self-correlation (see also Anderson (2009), Sorbjan and Grachev (2010) and Rodrigo and Anderson (2013)). They showed that Pr_t increases with increasing stability when it is plotted against R_g, but decreases with increasing stability when it is plotted against ζ or the flux Richardson number (R_f) using the same data collected during the Surface Heat Budget of the Arctic Ocean (SHEBA) experiment. Also using the SHEBA data, Sorbjan and Grachev (2010) found that Pr_t actually decreases from 0.9 under near-neutral conditions to about 0.7 under very stable conditions after removing outliers that seem to have large values of R_g but are actually caused by small temperature and velocity gradients under near-neutral conditions. Anderson (2009) employed regression methods to avoid self-correlation and found that Pr_t increases with increasing R_g consistent with Fig. 6(a). The issue of self-correlation, together with the disagreement among different studies, highlights the challenge of studying Pr_t with field data under stable conditions. Other complexities in stable boundary layers, including non-stationarity, wave-turbulence interaction, global intermittency and collapsing turbulence, are reviewed elsewhere and are not repeated here (Fernando and Weil, 2010; Mahrt, 2014; Sun et al., 2015).

Due to these experimental challenges and complexities associated with stable boundary layers (especially strongly stable boundary layers) in real-world settings, many investigations of Pr_t under stable conditions have focused on fully developed, stationary, and homogeneous boundary layers using theoretical approaches. Before these studies are reviewed, the asymptotical behaviors of Pr_t under near-neutral and very stable conditions, indicated by very small and large values of R_g, are first discussed.

6.1. Asymptotical behaviors

At very large R_g (i.e., under strongly stable conditions), the Pr_t is expected to increase nearly linearly with increasing R_g (see Fig. 6). This stems from the definition of $Pr_t = R_g/R_f$. At very large R_g, R_f tends to saturate or level off towards its maximum value (R_{fm}, hereafter called the maximum flux Richardson number), leading to Pr_t increasing linearly with R_g. This result is well supported by experimental data and numerical simulations (see Fig. 6a).

At very low R_g (i.e., under near-neutral conditions), different arguments exist. Schumann and Gerz (1995) noticed that Pr_t is fairly insensitive to stability at low R_g and proposed the following parameterization for Pr_t by merging the behaviors of Pr_t at very small and large R_g:

$$Pr_t = Pr_{t,neu}\, exp\left(-\frac{R_g}{Pr_{t,neu}R_{fm}}\right) + \frac{R_g}{R_{fm}} \tag{36}$$

On the other hand, Venayagamoorthy and Stretch (2010) argued that Pr_t should increase linearly with R_g at small R_g and proposed a modified empirical function for Pr_t, as follows:

$$Pr_t = Pr_{t,neu}\, exp\left(-\frac{R_g}{Pr_{t,neu}R_{fm}} + \frac{R_g}{Pr_{t,neu}}\right) + \frac{R_g}{R_{fm}} \tag{37}$$

Both functions agree with experimental data and numerical simulation results fairly well, as shown in Fig. 6(a). The minor difference between the two functions at small R_g is well within the scatter of experimental data and numerical simulation results. Besides the two functions constructed based on the asymptotic behaviors of Pr_t, other empirical and semi-empirical formulations that describe the behavior of Pr_t as a function of R_g under stable conditions also exist (Kondo et al., 1978; Louis et al., 1982; Kim and Mahrt, 1992; Zilitinkevich and Calanca, 2000; Aliabadi et al., 2016). These formulations often parameterize Pr_t as a linear function of R_g (Kim and Mahrt, 1992; Baas et al., 2008; Zilitinkevich et al., 2008; Grisogono, 2010; Aliabadi et al., 2016). Elliott and Venayagamoorthy (2011) evaluated four different Pr_t parameterizations for stably stratified turbulence, including the one proposed by Venayagamoorthy and Stretch (2010), and found considerable variability in the simulation results with different Pr_t parameterizations even in a one-dimensional channel flow.

6.2. Second-order turbulence closure models

Perhaps the most commonly-employed theoretical approach for studying Pr_t, as alluded to in Section 3.3, is to derive Pr_t from second-order (or even higher-order) turbulence closure models. In this section, the Pr_t under stable conditions from two representative second-order turbulence closure models, the classic Mellor-Yamada (MY) model (Mellor, 1973; Yamada, 1975; Mellor and Yamada, 1982) and the Energy- and Flux-Budget (EFB) model recently developed by Zilitinkevich et al. (2007, 2009, 2013), are discussed. These two models are selected because they represent two different situations distinguished by whether the model is subjected to the so-called 'critical gradient Richardson number' (R_{gc}). To simplify the comparison, the two models are applied to the idealized ASL where analytical expressions for Pr_t can be obtained (Li et al., 2016a).

6.2.1. Governing equations

Here the governing equations for second-order turbulence closure models are presented, which include the budget equations for turbulent momentum and heat fluxes (Eqs. (17) and (18)) already presented in Section 3.3. In addition, governing equations for $\overline{w'w'}$ and $\overline{\theta'\theta'}$ are needed to close the turbulent flux budget models, as can be seen from Eq. (25). In the idealized ASL, these are given by

$$\frac{\partial \overline{w'w'}}{\partial t} = 0 = 2\beta\overline{w'\theta'} - \frac{\partial \overline{w'w'w'}}{\partial z} - \frac{2}{\rho}\frac{\partial \overline{w'p'}}{\partial z} + 2\overline{\frac{p'}{\rho}\frac{\partial w'}{\partial z}} - 2\nu\overline{\left(\frac{\partial w'}{\partial z}\right)^2}, \tag{38}$$

$$\frac{\partial \overline{\theta'\theta'}}{\partial t} = 0 = -2\overline{w'\theta'}\Gamma - \frac{\partial \overline{w'\theta'\theta'}}{\partial z} - 2D_m\overline{\left(\frac{\partial \theta'}{\partial z}\right)^2} \tag{39}$$

The terms on the right hand-side of the equations represent (in order): production terms due to buoyancy for $\overline{w'w'}$ or due to the presence of mean temperature gradient (i.e., Γ) for $\overline{\theta'\theta'}$, turbulent transport terms, pressure-decorrelation terms due to interactions between pressure and velocity (which is absent for $\overline{\theta'\theta'}$), and molecular destruction or dissipation terms. The molecular destruction or dissipation terms in these two equations are extremely important and cannot be neglected as in the equations for $\overline{u'w'}$ and $\overline{w'T'}$ (Eqs. (17) and (18)).

Given that $\overline{u'u'}$ and $\overline{v'v'}$ do not directly affect the vertical momentum and heat fluxes in the idealized ASL, they do not need to be included when solving these budget equations. However, second-order closure schemes typically consider the total TKE equation or two separate equations for $\overline{u'u'}$ and $\overline{v'v'}$. Here, the budget equation for the total TKE, $\bar{e} = 0.5(\overline{u'u'} + \overline{v'v'} + \overline{w'w'})$, is presented for completeness:

$$\frac{\partial \bar{e}}{\partial t} = 0 = -\overline{u'w'}S + \beta\overline{w'\theta'} - \frac{\partial \overline{w'e}}{\partial z} - \frac{1}{\rho}\frac{\partial \overline{w'p'}}{\partial z} - \varepsilon \tag{40}$$

Again, the terms on the right hand-side of the equation represent (in order): the production term due to shear, the production or destruction term due to buoyancy, the turbulent transport term, the pressure-decorrelation term due to interactions between pressure and velocity, and the dissipation term.

Note that in Section 3.3 we have neglected $\overline{u'\theta'}$ in the momentum flux budget equation. When $\overline{u'\theta'}$ is not neglected, the governing equation for $\overline{u'\theta'}$ needs to be also provided in order to close the equation system (Mellor, 1973; Yamada, 1975).

6.2.2. The Mellor-Yamada (MY) model

For over four decades now, the Mellor-Yamada (MY) model (Mellor and Yamada, 1982) and its many variants have been widely used in studying geophysical turbulence. The key parameterization used in the MY model is the Rotta scheme (Rotta, 1951) for pressure decorrelation terms, which can involve one (Mellor, 1973) or three (Yamada, 1975) or even more (Nakanish, 2001) coefficients depending on the complexity of the Rotta scheme (see Eqs. (21) and (22) for the simplest Rotta scheme that only retains the slow component and has one coefficient). In addition, the MY model employs four length scales (two are relaxation length scales in the Rotta model and two are dissipative length scales for parameterizing the dissipation rates of variances), all of which are assumed to be proportional to the so-called master length scale. To match expectations from a neutral ASL, the master length scale is set to be κz, where κ is again the von Kármán constant and z is the height above the ground. As a result, the MY model requires five (Mellor, 1973) or seven (Yamada, 1975) empirical constants, which were obtained by fitting to observational data collected in the ASL.

The MY model includes a hierarchy of closure schemes and the level 2 scheme, which is discussed here, further neglects the third-order turbulent transport terms in all equations for second-order statistics. With this additional assumption, the set of equations can be solved analytically as shown in Mellor (1973) and Yamada (1975). The Pr_t from Yamada (1975) is reproduced here, as follows:

$$Pr_t = Pr_{t,neu}\left(\frac{1 - R_f/R_{f2}}{1 - R_f/R_{f1}}\right)^{-1}, \tag{41}$$

where $Pr_{t,\ neu} = 0.74$, $R_{f1} = 0.325$, $R_{f2} = 0.316$ are constants derived from the previously mentioned basic constants.

6.2.3. The energy- and flux-budget (EFB) model

The main differences between the EFB model and the MY model have been discussed in Li et al. (2016a) and thus are not repeated here. Similar to the MY model, the EFB model has several basic constants that need to be determined a priori. Results from the most recent version of the EFB model (Zilitinkevich et al., 2013) are presented here, where the turbulent Prandtl number is given by

$$Pr_t = Pr_{t,neu}\left(1 - \frac{R_f}{1 - R_f}\frac{(1 - R_{fm})}{R_{fm}}\frac{A_z^{\infty}}{A_z}\right)^{-1}, \tag{42}$$

where $Pr_{t,\ neu} = 0.8$ and $R_{fm} = 0.25$ are derived from the basic constants of the EFB model (Zilitinkevich et al., 2013). The $A_z = \overline{w'w'}/\bar{e}$ is the vertical anisotropy (i.e., the vertical component of the TKE normalized by the total TKE) given by

$$A_z = \frac{C_r^{efb}\left(1 - 2C_o^{efb}\frac{R_f}{R_{fm}}\right)(1 - R_f) - 3R_f}{(1 - R_f)\left(3 + C_r^{efb}\left(3 - 2(1 + C_o^{efb})\frac{R_f}{R_{fm}}\right)\right)}, \tag{43}$$

where C_r^{efb} (=1.5) is a standard inter-component energy exchange constant and C_o^{efb} (=0.125) is the inter-component energy exchange constant determining the vertical share of TKE. The constant A_z^{∞} (=0.03) is the value of A_z at $R_g \to \infty$.

6.2.4. Comparison between the MY model and the EFB model

The comparison between the MY and EFB models is presented in Fig. 6(b) so that they can also be compared to experimental data and numerical simulation results shown in Fig. 6(a). The major difference between the MY and EFB models is that the MY model only works when the gradient Richardson number is smaller than the so-called 'critical gradient Richardson number' (R_{gc}), which is about 0.2–0.25. This 'critical gradient Richardson number' is often interpreted as the threshold characterizing laminar-turbulent transition in stably stratified flows, which originates from the seminal work of Miles and Howard (Miles, 1961; Howard, 1961). Beyond this value, turbulence collapses and the Pr_t is not well defined in the MY model (see Fig. 6b).

On the other hand, the EFB model predicts the linear increase in Pr_t at sufficiently large R_g and does not support the concept of 'critical gradient Richardson number'. In essence, the EFB model argues that R_g depends only on the mean flow state and increases in R_g are not limited by the internal turbulence state (i.e. the ability of turbulence to transport momentum and heat) (Zilitinkevich et al., 2013). As such, the EFB model treats the vertical gradients of mean velocity and temperature as 'external' variables to the turbulent flux budgets. By virtue of this treatment, the EFB model is not limited by a 'critical gradient Richardson number'.

However, unlike R_g depending on the 'external' mean velocity and temperature gradients, R_f is controlled by the 'internal' turbulence state and thus cannot increase indefinitely as R_g increases. The EFB model caps the R_f through imposing a maximum value or R_{fm} derived from observational data, which is around 0.2–0.25 (Zilitinkevich et al., 2013). It should be noted that there are experimental studies reporting values of R_f larger than 0.25 and sometimes even larger than unity (Pardyjak et al., 2002) probably because of non-stationarity, advection, and flux transport.

The existence of a 'critical gradient Richardson number' continues to be a topic receiving attention in turbulence modeling (Canuto et al., 2008; Ferrero et al., 2011), but experimental evidence, shown in Fig. 6 and elsewhere (Galperin et al., 2007), favors no such threshold. Recently, Grachev et al. (2013) found that the 'critical gradient Richardson number' in the ASL indicates a threshold beyond which MOST does not apply and, coincidentally, the inertial subrange in the Richardson-Kolmogorov energy cascade dies out (see also Li et al. (2015a)). This has motivated new investigations of connections between the mean flow properties described by MOST and the eddy structures characterized by the inertial subrange scaling, as shall be examined in Section 7.

6.3. The Quasi-Normal Scale Elimination (QNSE) model

A different theoretical approach to stably stratified turbulence is the Quasi-Normal Scale Elimination (QNSE) model (Sukoriansky et al., 2005a, 2005b, 2006; Galperin and Sukoriansky, 2010). The QNSE model is a spectral closure that gradually coarsens the resolved scales by successively eliminating the unresolved scales. When this process of successive averaging is extended to the largest turbulent scale, the QNSE theory yields a RANS model that includes eddy viscosities and diffusivities in both horizontal and vertical directions. Details of the QNSE model (Sukoriansky et al., 2005a, 2005b, 2006; Galperin and Sukoriansky, 2010) and its implementation into numerical weather prediction models (Tastula et al., 2015a, 2015b, 2016) can be found elsewhere.

There is no analytical expression for Pr_t from the QNSE model. Fig. 6(b) shows the Pr_t inferred from the fitted functions of ϕ_m and ϕ_h in the QNSE model (Tastula et al., 2015b). Although the Pr_t from the QNSE model is lower than those from the other models, it captures the linear increase of Pr_t with R_g at large R_g values. Similar to the EFB model, the Pr_t from the QNSE model is not subjected to a 'critical

gradient Richardson number'.

7. A unifying framework for Pr_t based on cospectral budgets

The above two sections have discussed recent advances in our understanding of Pr_t under unstable and stable conditions, respectively. The phenomenological model presented in Section 5 shows a strong linkage between the mean velocity and temperature profiles in an unstable ASL and the Kolmogorov scaling in the inertial subrange (Li et al., 2012b). In stable conditions, experimental data suggest that the 'critical gradient Richardson number' is tied to the collapse of inertial subrange in the Richardson-Kolmogorov energy cascade (Grachev et al., 2013; Li et al., 2015a). Collectively they seem to suggest that there are close connections between the mean flow properties, including the mean velocity and temperature profiles and thus Pr_t, and the microscale turbulent energy distributions governed by the inertial subrange scaling. Such connections are formally established by a recently developed cospectral budget (CSB) model (Katul et al., 2013a, 2014; Li et al., 2015a, 2015b), which provides a unifying framework for Pr_t in the ASL. Given its significance, the detailed derivation of Pr_t in the CSB model (Li et al., 2015b) is reproduced here.

7.1. Model formulations

The CSB framework starts with the cospectral definitions of turbulent momentum and heat fluxes:

$$\overline{u'w'} = \int_0^\infty F_{uw}(k)dk \tag{44}$$

$$\overline{w'\theta'} = \int_0^\infty F_{w\theta}(k)dk, \tag{45}$$

where $F_{uw}(k)$ and $F_{w\theta}(k)$ are the co-spectra of w' and u', and w' and θ', respectively, and k is a one-dimensional wavenumber in the streamwise direction. This definition of k is used in order to be consistent with ASL experiments that typically report spectra and co-spectra from single-point time series measurements (Kaimal et al., 1972; Kaimal, 1973; Kaimal and Finnigan, 1994; Wyngaard and Cote, 1972) based on Taylor's frozen turbulence hypothesis (Taylor, 1938).

In correspondence to the budgets of turbulent momentum and heat fluxes (Eqs. (17) and (18) in Section 3.3), the cospectral budgets of momentum and heat fluxes in an idealized ASL can be simplified as follows (Panchev, 1971; Bos et al., 2004; Bos and Bertoglio, 2007; Canuto et al., 2008; Katul et al., 2013a):

$$0 = P_{uw}(k) + T_{uw}(k) + \pi_u(k) + \beta F_{u\theta}(k) - 2\nu k^2 F_{uw}(k), \tag{46}$$

$$0 = P_{w\theta}(k) + T_{w\theta}(k) + \pi_\theta(k) + \beta F_{\theta\theta}(k) - (\nu + D_m)k^2 F_{w\theta}(k) \tag{47}$$

The terms on the right hand-side of the equations represent (in order): production (P), flux-transfer (T), pressure-decorrelation (π), buoyancy ($\beta F_{u\theta}$ and $\beta F_{\theta\theta}$), and molecular destruction. $F_{u\theta}$ is the co-spectra of u' and θ' and $F_{\theta\theta}(K)$ is the spectrum of potential temperature. Similar to the arguments presented in Section 3.3, the molecular destruction terms are assumed to be small. This is equivalent to assuming that eddies whose sizes are on the order of the Kolmogorov microscale η (on the order of 1 mm) do not contribute significantly to momentum and heat fluxes, at least when compared to other mechanisms. The $F_{u\theta}(k)$ term is also assumed to be small compared to $P_{uw}(k)$ as demonstrated by DNS results (Katul et al., 2014; Shah and Bou-Zeid, 2014b) and scaling arguments (Stull, 1988). Note that in Section 3.3, the third-order flux-transport terms are also neglected. However, it is important to point out that here the 'flux-transfer' term in the spectral space is different from the 'flux-transport' term in the physical space and in the context of Reynolds-averaged equation. While the flux-transport terms may be negligible in the idealized ASL, the flux-transfer terms can be significant at any given k.

Hence, the simplified cospectral budgets of momentum and heat fluxes are given by:

$$P_{uw}(k) + T_{uw}(k) + \pi_u(k) = 0, \tag{48}$$

$$P_{w\theta}(k) + T_{w\theta}(k) + \pi_\theta(k) + \beta F_{\theta\theta}(k) = 0 \tag{49}$$

The production terms can be obtained from direct Fourier transforming $-\overline{w'w'}\mathrm{S}$ and $-\overline{w'w'}\Gamma$:

$$P_{uw}(k) = -F_{ww}(k)\mathrm{S}, \tag{50}$$

$$P_{w\theta}(k) = -F_{ww}(k)\Gamma, \tag{51}$$

where $F_{ww}(k)$ is the vertical velocity spectrum.

The flux-transfer terms act to move fluxes away from the peak of the co-spectra and hence they can be parameterized using a spectral gradient-diffusion model as (Bos et al., 2004; Bos and Bertoglio, 2007):

$$T_{uw}(k) = -A_{UU}\frac{\partial}{\partial k}(\varepsilon^{1/3}\,k^{5/3}F_{uw}(k)), \tag{52}$$

$$T_{w\theta}(k) = -A_{\theta\theta}\frac{\partial}{\partial k}(\varepsilon^{1/3}\,k^{5/3}F_{w\theta}(k)), \tag{53}$$

where A_{UU} and $A_{\theta\theta}$ are model constants associated with the flux-transfer terms and ε is again the mean dissipation rate of TKE.

To model the pressure de-correlation terms, a Rotta-type parameterization is invoked in the spectral domain, which corresponds to the one widely used in the previously discussed second-order closure schemes (Mellor and Yamada, 1974; Yamada, 1975). Specifically, the following closure formulations are employed (Launder et al., 1975; Pope, 2000):

$$\pi_u(k) = -A_U\frac{F_{uw}(k)}{\tau_u(k)} - C_{IU}P_{uw}(k), \tag{54}$$

$$\pi_\theta(k) = -A_\theta\frac{F_{w\theta}(k)}{\tau_\theta(k)} - C_{I\theta}P_{w\theta}(k), \tag{55}$$

where A_U and A_θ (≈ 1.8) are the Rotta constants (Pope, 2000), $C_{I\theta}$ and C_{IU} ($\approx 3/5$) are constants associated with isotropization of production terms (called isotropization constants hereafter), which can be determined using the Rapid Distortion Theory in homogeneous turbulence (Pope, 2000). The $\tau_u(k)$ and $\tau_\theta(k)$ are wavenumber-dependent relaxation time scales for momentum and heat fluxes, respectively. A widely used formulation for $\tau_u(k)$ and $\tau_\theta(k)$ are given by (Corrsin, 1961; Bos et al., 2004; Bos and Bertoglio, 2007; Cava and Katul, 2012; Katul et al., 2014):

$$\tau_u(k) = \tau_\theta(k) = \varepsilon^{-1/3}k^{-2/3} \tag{56}$$

With these parameterizations, Eqs. (48) and (49) reduce to:

$$\frac{\partial F_{uw}(k)}{\partial k} + \left(\frac{A_U}{A_{UU}} + \frac{5}{3}\right)k^{-1}F_{uw}(k) = -\frac{(1-C_{IU})}{A_{UU}\varepsilon^{1/3}}\mathrm{S}F_{ww}(k)k^{-5/3}, \tag{57}$$

$$\frac{\partial F_{w\theta}(k)}{\partial k} + \left(\frac{A_\theta}{A_{\theta\theta}} + \frac{5}{3}\right)k^{-1}F_{w\theta}(k) = -\frac{(1-C_{I\theta})}{A_{\theta\theta}\varepsilon^{1/3}}\Gamma F_{ww}(k)k^{-5/3} + \frac{\beta}{A_{\theta\theta}\varepsilon^{1/3}}F_{\theta\theta}(k)k^{-5/3} \tag{58}$$

The above equations for $F_{uw}(k)$ and $F_{w\theta}(k)$ can be solved once $F_{ww}(k)$ and $F_{\theta\theta}(k)$ are known or specified. The precise spectral shapes of $F_{ww}(k)$ and $F_{\theta\theta}(k)$ used by the CSB model will be discussed later. However, for illustration purposes, it is convenient to begin with a single power-law formulation with $F_{ww}(k) = C_{ww}k^{-\alpha}$ and $F_{\theta\theta}(k) = C_{\theta\theta}k^{-\gamma}$, where α and γ are spectral scaling exponents and C_{ww} and $C_{\theta\theta}$ are normalization factors. With these expressions for $F_{ww}(k)$ and $F_{\theta\theta}(k)$, Eqs. (57) and (58) reduce to two uncoupled, first-order ordinary differential equations given as:

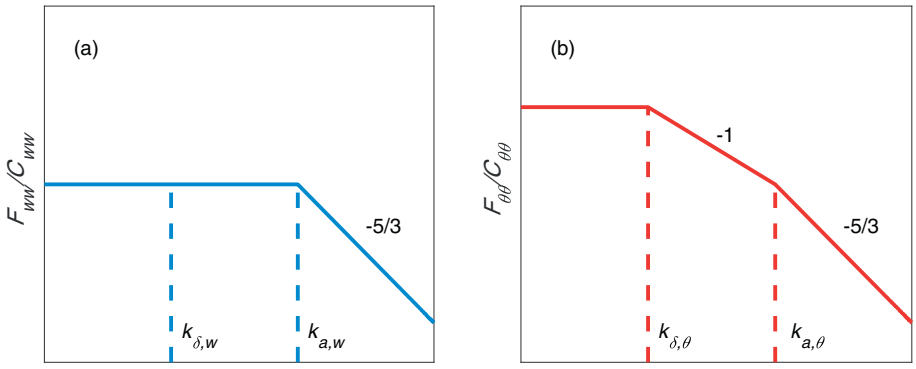

Fig. 7. The idealized shapes of (a) F_{ww} and (b) $F_{\theta\theta}$.

$$\frac{dF_{uw}(k)}{dk} + D_1 k^{-1} F_{uw}(k) = D_2 C_{ww} k^{-\alpha-5/3}, \tag{59}$$

$$\frac{dF_{w\theta}(k)}{dk} + D_3 k^{-1} F_{w\theta}(k) = D_4 C_{ww} k^{-\alpha-5/3} + D_5 C_{\theta\theta} k^{-\gamma-5/3} \tag{60}$$

where $D_1 = A_U/A_{UU} + 5/3$, $D_2 = -(1 - C_{IU})S/(A_{UU}\varepsilon^{1/3})$, $D_3 = A_\theta/A_{\theta\theta} + 5/3$, $D_4 = -(1 - C_{I\theta})\Gamma/(A_{\theta\theta}\varepsilon^{1/3})$, and $D_5 = \beta/(A_{\theta\theta}\varepsilon^{1/3})$. These two equations can be solved to yield:

$$F_{uw}(k) = \frac{D_2}{-\alpha - 2/3 + D_1} C_{ww} k^{-\alpha-2/3} + E_1 k^{-D_1}, \tag{61}$$

$$F_{w\theta}(k) = \frac{D_4}{-\alpha - 2/3 + D_3} C_{ww} k^{-\alpha-2/3} + \frac{D_5}{-\gamma - 2/3 + D_3} C_{\theta\theta} k^{-\gamma-2/3} + E_2 k^{-D_3}, \tag{62}$$

where E_1 and E_2 are integration constants to be determined later.

7.2. Idealized spectral shapes of $F_{ww}(k)$ and $F_{\theta\theta}(k)$

Eqs. (61) and (62) can be integrated across all k to obtain turbulent momentum and heat fluxes in the physical space. This, however, requires $F_{ww}(k)$ and $F_{\theta\theta}(k)$ as inputs. As a compromise between realistic spectral shapes in the ASL and the need for analytical tractability, previous studies often used multi-exponent approximations to $F_{ww}(k)$ and $F_{\theta\theta}(k)$ (Katul et al., 2013a, 2014; Li et al., 2015a, 2015b). Nonetheless, the exact formations of the multi-exponent approximations to $F_{ww}(k)$ and $F_{\theta\theta}(k)$ differed among studies (Katul et al., 2013a, 2014; Li et al., 2015a, 2015b).

To ensure maximum flexibility, both $F_{ww}(k)$ and $F_{\theta\theta}(k)$ are assumed to compose of three parts here (see Fig. 7): the very low frequency part ($k < k_\delta$, where k_δ is the wavenumber corresponding to the ABL height), the low frequency part ($k_a < k < k_\delta$, where k_a is the wavenumber corresponding to the height above the surface and delineating attached eddies from detached eddies), and the high frequency part ($k > k_a$). The high frequency part is assumed to follow the Kolmogorov '-5/3' power law scaling (Kolmogorov, 1941). The low frequency part is designed to capture the '-1' power law scaling for $F_{\theta\theta}(k)$ but not for $F_{ww}(k)$, as suggested by several ASL experiments (Kader and Yaglom, 1991; Katul et al., 1995; Katul and Chu, 1998; Li et al., 2015a) and recent DNS results (McColl et al., 2017). Both spectra are assumed to become invariant with k in the very low frequency part to accommodate energy associated with very-large scale motions and superstructures (Guala et al., 2010; Hutchins et al., 2012; Marusic et al., 2010; Smits et al., 2011). The following functions summarize the idealized forms for $F_{ww}(k)$ and $F_{\theta\theta}(k)$:

$$F_{ww}(K) = \begin{cases} C_{ww_1} k^{-\alpha_1}, & k < k_{\delta,w} \\ C_{ww_2} k^{-\alpha_2}, & k_{\delta,w} < k < k_{a,w} \\ C_{ww_3} k^{-\alpha_3}, & k > k_{a,w} \end{cases} \tag{63}$$

$$F_{\theta\theta}(k) = \begin{cases} C_{\theta\theta_1} k^{-\gamma_1}, & k < k_{\delta,\theta} \\ C_{\theta\theta_2} k^{-\gamma_2}, & k_{\delta,\theta} < k < k_{a,\theta} \\ C_{\theta\theta_3} k^{-\gamma_3}, & k > k_{a,\theta} \end{cases} \tag{64}$$

where $\alpha_1 = 0$, $\gamma_1 = 0$, $\alpha_2 = 0$, $\gamma_2 = 1$, and $\alpha_3 = \gamma_3 = 5/3$. The values of C_{ww_3} and $C_{\theta\theta_3}$ can be determined from Kolmogorov's theory (Kolmogorov, 1941): $C_{ww_3} = C_o\varepsilon^{2/3}$ and $C_{\theta\theta_3} = C_T N_T \varepsilon^{-1/3}$, where C_o and C_T are the Kolmogorov and the Kolmogorov-Obukhov-Corrsin phenomenological constants, respectively, whose values are $C_o = 0.65$ and $C_T = 0.8$ when k is a one-dimensional wavenumber (Ishihara et al., 2002; Chung and Matheou, 2012). The N_T is the mean temperature variance dissipation rate. The values of C_{ww_2}, C_{ww_1}, $C_{\theta\theta_2}$ and $C_{\theta\theta_1}$ are then determined from continuity constraints (e.g., $C_{ww_3}k_{a,\ w}{}^{-\alpha_3} = C_{ww_2}k_{a,\ w}{}^{-\alpha_2}$ and $C_{ww_2}k_{\delta,\ w}{}^{-\alpha_2} = C_{ww_1}k_{\delta,\ w}{}^{-\alpha_1}$). It should be pointed out that the idealized forms for $F_{ww}(k)$ and $F_{\theta\theta}(k)$ used here are slightly different from those in previous studies (Katul et al., 2013a, 2014; Li et al., 2015a, 2015b).

7.3. The integration constants E_1 and E_2

Besides the spectral shapes of $F_{ww}(k)$ and $F_{\theta\theta}(k)$, the integration constants (i.e., E_1 and E_2) are also required to evaluate $F_{uw}(k)$ and $F_{w\theta}(k)$. They are simply assumed to be zero, which yield a '-7/3' scaling in the inertial subrange of $F_{uw}(k)$ and $F_{w\theta}(k)$. This is supported by experimental studies that reported '-7/3' power law scalings in the inertial subrange of momentum and heat flux co-spectra (Kaimal and Finnigan, 1994; Saddoughi and Veeravalli, 1994), and is also consistent with previous dimensional analysis (Lumley, 1964). However, anomalous scaling for $F_{uw}(k)$ and $F_{w\theta}(k)$ have been reported in the ASL (Li and Katul, 2017) and in the canopy sublayer (Cava and Katul, 2012). Deviations of E_2 from zero will be later examined in Section 8.

7.4. Results

Using the idealized spectral shapes of $F_{ww}(k)$ and $F_{\theta\theta}(k)$ and the assumption of $E_1 = E_2 = 0$, Eqs. (44) and (45) can now be evaluated.

$$\overline{u'w'} = \int_0^\infty F_{uw}(k)dk = f_1 D_2 C_o \varepsilon^{2/3}, \tag{65}$$

$$\overline{w'\theta'} = \int_0^\infty F_{w\theta}(k)dk = g_1 D_4 C_o \varepsilon^{2/3} Q, \tag{66}$$

where

$$Q = 1 - \omega_1 \frac{\zeta}{\phi_m - \zeta}, \tag{67}$$

$$\omega_1 = \frac{1}{(1 - C_{I\theta})} \frac{C_T}{C_o} \frac{g_2}{g_1}, \tag{68}$$

$$f_1 = \frac{1}{(-\alpha_1 - 2/3 + D_1)(-\alpha_1 + 1/3)} k_{\delta,w}^{-\alpha_2+1/3} k_{a,w}^{\alpha_2-\alpha_3} + \frac{1}{(-\alpha_2 - 2/3 + D_1)(-\alpha_2 + 1/3)} (k_{a,w}^{-\alpha_3+1/3} - k_{\delta,w}^{-\alpha_2+1/3} k_{a,w}^{\alpha_2-\alpha_3}) + \frac{1}{(-\alpha_3 - 2/3 + D_1)(-\alpha_3 + 1/3)} (-k_{a,w}^{-\alpha_3+1/3}), \quad (69)$$

$$g_1 = \frac{1}{(-\alpha_1 - 2/3 + D_3)(-\alpha_1 + 1/3)} k_{\delta,w}^{-\alpha_2+1/3} k_{a,w}^{\alpha_2-\alpha_3} + \frac{1}{(-\alpha_2 - 2/3 + D_3)(-\alpha_2 + 1/3)} (k_{a,w}^{-\alpha_3+1/3} - k_{\delta,w}^{-\alpha_2+1/3} k_{a,w}^{\alpha_2-\alpha_3}) + \frac{1}{(-\alpha_3 - 2/3 + D_3)(-\alpha_3 + 1/3)} (-k_{a,w}^{-\alpha_3+1/3}), \quad (70)$$

$$g_2 = \frac{1}{(-\gamma_1 - 2/3 + D_3)(-\gamma_1 + 1/3)} k_{\delta,\theta}^{-\gamma_2+1/3} k_{a,\theta}^{\gamma_2-\gamma_3} + \frac{1}{(-\gamma_2 - 2/3 + D_3)(-\gamma_2 + 1/3)} (k_{a,\theta}^{-\gamma_3+1/3} - k_{\delta,\theta}^{-\gamma_2+1/3} k_{a,\theta}^{\gamma_2-\gamma_3}) + \frac{1}{(-\gamma_3 - 2/3 + D_3)(-\gamma_3 + 1/3)} (-k_{a,\theta}^{-\gamma_3+1/3}). \quad (71)$$

To obtain the above expressions, local balances between production and dissipation terms in the TKE and potential temperature variance budgets have been assumed (Katul et al., 2014). In addition, the above integration implicitly assumes that the vertical gradients of mean velocity and temperature are independent of wavenumber. That is, the mean velocity and temperature gradients are essentially viewed as being 'imposed' by the mean flow on turbulence (similar to the EFB model).

From Eqs. (65) and (66), one can obtain

$$Pr_t = Pr_{t,neu} Q^{-1} = Pr_{t,neu} \left(1 - \omega_1 \frac{\zeta}{\phi_m - \zeta}\right)^{-1} \quad (72)$$

where $Pr_{t,\ neu}$ is the turbulent Prandtl number when $\zeta = 0$ (i.e., under neutral conditions)

$$Pr_{t,neu} = \frac{A_{\theta\theta}}{A_{UU}} \frac{1 - C_{IU}}{1 - C_{I\theta}} \frac{f_1}{g_1}, \quad (73)$$

and Q represents the stability effects on the turbulent Prandtl number. To ensure a down-gradient sensible heat flux, Q needs to be larger than 0.

In addition to the stability parameter ζ, the flux Richardson number (R_f) and gradient Richardson number (R_g) are also widely used to indicate the thermal stratification or the stability effect as mentioned before. The Pr_t can be formulated as a function of the flux Richardson number R_f as follows:

$$Pr_t = Pr_{t,neu} \left(1 - \omega_1 \frac{R_f}{1 - R_f}\right)^{-1} \quad (74)$$

Given that the $Pr_t = R_g/R_f$, Pr_t can be also expressed as a function of R_g as follows:

$$Pr_t = Pr_{t,neu} \left[\frac{1 + \omega_2 R_g - \sqrt{-4R_g + (-1 - \omega_2 R_g)^2}}{2R_g}\right]^{-1}, \quad (75)$$

where $\omega_2 = \omega_1 + 1$.

7.5. Discussions

7.5.1. The Pr_t - stability relations

Before presenting the Pr_t - stability relations from the CSB model and comparing them to observational data and other models, it is important to examine the analytical expressions (Eqs. (72), (74), and (75)), which illustrate the controlling parameters of the Pr_t - stability relations. Assuming that the stability correction function ϕ_m is given by the Businger form (Businger et al., 1971), the dependence of Pr_t on ζ is then only controlled by ω_1 (see Eq. (68)), namely, by the ratio of the Kolmogorov-Obukhov-Corrsin to the Kolmogorov phenomenological constants (C_T/C_o), a constant associated with isotropization of the production term in the cospectral budget of heat ($C_{I\theta}$), and the ratio of g_2/g_1 encoding the spectral shapes of vertical velocity and potential temperature. The Kolmogorov and the Kolmogorov-Obukhov-Corrsin phenomenological constants have been investigated extensively in the literature and are believed to be near universal (Sreenivasan, 1995, 1996; Yeung and Zhou, 1997). The isotropization constant for homogeneous turbulence can be determined from Rapid Distortion Theory as 3/5 (Pope, 2000). Therefore, when the spectral shapes of vertical velocity and air temperature are identical so that $g_2/g_1 = 1$ (i.e., when the '-1' scaling does not exist), the $Pr_t - \zeta$ relation (and also the $Pr_t - R_f$ and $Pr_t - R_g$ relations) is only controlled by two universal phenomenological constants (namely, C_T/C_o and $C_{I\theta}$). This remarkable result suggests that the universality in the Pr_t - stability relations in the idealized ASL, which are often described by MOST, is inherited from the universal Kolmogorov scaling in the inertial subrange, thereby proving that there are strong linkages between macroscopic flow features in the logarithmic region of wall-bounded turbulent boundary layers and eddy structures in the inertial subrange (Gioia et al., 2010; Katul et al., 2013a, 2013b, 2014; Li et al., 2012b; Zúñiga-Zamalloa et al., 2014; Katul and Manes, 2014).

7.5.2. Comparison with other models

The $Pr_t - \zeta$ relation under unstable condition predicted by the CSB model (when $g_2/g_1 = 1$) is shown in Fig. 3, which is broadly consistent with previous studies considering the uncertainties of experimental data. However, it should be pointed out that such a relation is significantly modulated by the existence of '-1' scaling in the temperature spectra (McColl et al., 2017) and other spectral features not considered here (Kader and Yaglom, 1991), as discussed in Li et al. (2015b).

The prediction of the $Pr_t - R_g$ relation under stable conditions (when $g_2/g_1 = 1$) is shown in Fig. 6(b). It can be seen that the CSB model predicts an increase in Pr_t as R_g increases, which is in good agreement with the EFB model result. However, despite the agreement on the $Pr_t - R_g$ relation, Eqs. (42) and (74) reveal fundamental differences between the EFB and CSB models.

First, the maximum flux Richardson number value is determined a priori from observations in the EFB model but is inferred from two phenomenological constants, namely, the ratio of C_T/C_o and $C_{I\theta}$, in the CSB model. Specifically, the R_{fm} can be inferred from Eq. (74) in the CSB model with the condition $Pr_t > 0$:

$$R_f < R_{fm} = \frac{1}{1 + \frac{1}{1 - C_{I\theta}} \frac{C_T}{C_o}} \approx 0.25 \quad (76)$$

It is interesting to observe that the CBS model yields a R_{fm} value that is consistent with the value used in the EFB model and other studies reviewed elsewhere (Katul et al., 2014). This suggests that the maximum flux Richardson number should be interpreted as a threshold above which the idealized shapes of the vertical velocity and temperature spectra, especially the Kolmogorov inertial subrange scaling, break down (Grachev et al., 2013; Li et al., 2015a), instead of a threshold indicating the laminarization of turbulent flows.

Second, combining Eqs. (74) and (76), the turbulent Prandtl number in the CSB model can be re-written as

$$Pr_t = Pr_{t,neu} \left(1 - \frac{R_f}{1 - R_f} \frac{1 - R_{fm}}{R_{fm}}\right)^{-1} \quad (77)$$

Comparing Eqs. (77) to (42) reveals that the vertical anisotropy (A_z) is the main difference between the CSB and EFB models in terms of modeling Pr_t. The CSB model is mathematically equivalent to the EFB model only if $A_z^{\infty}/A_z = 1$. Note that the factor A_z^{∞}/A_z is close to unity at strong stratification but deviates from unity at weak stratification.

Despite this difference, however, both models agree in their turbulent Prandtl number predictions across a wide range of stability. This is because the multiplier $R_f/(1-R_f)$ is small at weak stratification. Even though A_z^{∞}/A_z deviates from unity at weak stratification, it does not induce significant changes in the predicted turbulent Prandtl number.

8. The subgrid-scale Prandtl number for LES

The discussions so far have been focused on the Pr_t for RANS modeling. As mentioned in the introduction, LES has become a widely-used numerical technique for studying the ABL flow and turbulence in general. The essence of LES is to resolve the large scales and to parameterize the effects of small scales using so-called subgrid-scale (SGS) models (Pope, 2000). The very high Reynolds number of the ABL implies a wide scale-separation between the large scales and the smallest scale (i.e., the Kolmogorov microscale) and hence provides a good testbed for LES. The separation between the large scales and the subgrid scales is achieved through some filtering operation, which is denoted by the tilde $(\sim)$ in order to be separated from the overbar $(-)$ indicating Reynolds averaging.

Employing the same local flux-gradient relation as in RANS closure schemes (Eqs. (3) and (4)), the SGS turbulent momentum (τ_{ij}) and heat (h_i) fluxes are modeled as

$$\tau_{ij} = -2c_s^2\Delta^2|\widetilde{S}|\widetilde{S}_{ij}, \tag{78}$$

$$h_i = -Pr_{SGS}^{-1}\, c_s^2\Delta^2|\widetilde{S}|\widetilde{D}_i, \tag{79}$$

respectively, where i and j indicate directions (e.g., u_i is the velocity in the i direction) and repeated indices imply summation, Δ is the filter scale, $|\widetilde{S}| = (2\widetilde{S}_{ij}\widetilde{S}_{ij})^{1/2}$, $\widetilde{S}_{ij} = 0.5(\partial\widetilde{u}_i/\partial x_j + \partial\widetilde{u}_j/\partial x_i)$, $\widetilde{D}_i = \partial\widetilde{\theta}/\partial x_i$, c_s is the Smagorinsky coefficient, and Pr_{SGS} is the SGS Prandtl number (the equivalent of Pr_t).

8.1. Early derivations and empirical models

Early derivations of the SGS Prandtl number were built on the determination of the Smagorinsky coefficient for isotropic turbulence (Lilly, 1967) and can be found in many studies (Schumann et al., 1980; Moeng and Wyngaard, 1988; Mason, 1989). By assuming that the inertial subrange spectra of TKE ($F_{TKE} = C_{TKE}\varepsilon^{2/3}k^{-5/3}$, where C_{TKE} is the Kolmogorov constant for TKE) and potential temperature ($F_{\theta\theta} = C_T\varepsilon^{-1/3}N_T k^{-5/3}$) apply to the wavenumber range of 0 to k_Δ $(=\pi/\Delta)$, one arrives:

$$\widetilde{S}^2 = 2\int_0^{k_\Delta} k^2F_{TKE}(k)dk = \frac{3}{2}C_{TKE}\varepsilon^{2/3}k_\Delta^{4/3}, \tag{80}$$

$$\widetilde{D}^2 = 2\int_0^{k_\Delta} k^2F_{\theta\theta}(k)dk = \frac{3}{2}C_T\varepsilon^{-1/3}N_T k_\Delta^{4/3}, \tag{81}$$

where $|\widetilde{D}| = (\widetilde{D}_i\widetilde{D}_i)^{1/2}$. It is pointed out here that the original work of Kolmogorov assumed that ϵ is the dissipation rate of the ensemble mean TKE, but here ϵ (and N_T) is the dissipation rate for the SGS TKE (and temperature variance). Assuming that the SGS TKE and temperature variance budgets are also in equilibrium and neglecting the effect of thermal stratification, one can show that $\epsilon/N_T = Pr_{SGS}\widetilde{S}^2/\widetilde{D}^2$ (Schumann et al., 1980; Moeng and Wyngaard, 1988; Mason, 1989). As such,

$$Pr_{SGS} = \frac{C_T}{C_{TKE}} \approx 0.47 \tag{82}$$

It is clear that the above derivation results in a Pr_{SGS} that is independent of stability and the filter scale (Δ) or the cut-off wavenumber (k_Δ). The value of $Pr_{SGS} = 0.47$ seems to be also lower than its RANS counterpart under neutral conditions (which is about $0.7 \sim 0.9$), suggesting a stronger (maybe excessive) mixing for heat (de Roode et al., 2017). A few studies considered the effect of thermal stratification on Pr_{SGS} but often in an ad-hoc way. Deardorff (1973, 1980) used a Pr_{SGS} that gradually increases from 1/3 under unstable and neutral conditions to 1 under very stable conditions based on heuristic arguments. Recently, Gibbs and Fedorovich (2016) chose to allow the transition of Pr_{SGS} from 1/3 to 1 to occur in the unstable regime instead of the stable regime as in Deardorff (1973, 1980). Others used empirical functions to account for the stability effect on Pr_{SGS} (Brown et al., 1994; Mason and Brown, 1999). Schumann (1991) solved the SGS momentum and heat flux budgets algebraically in the physical space (similar to the MY model for RANS modeling), which yielded a Pr_{SGS} that increases with the stable stratification. None of these studies, however, considered the variation of Pr_{SGS} with the filter scale (Δ), which may occur near the surface where the filter scale falls outside of the inertial subrange.

8.2. Observations and dynamic model results

Laboratory and field experimental data are critical for addressing the issue of stability- and scale-dependence of Pr_{SGS}. Laboratory investigations in the wake of a heated cylinder obtained a value of about 0.3 for Pr_{SGS} under neutral conditions (Kang and Meneveau, 2002). In the ASL, direct determination of Pr_{SGS} benefited from a series of Horizontal Arrays Turbulence Study (HATS)-type experiments (Horst et al., 2004; Bou-Zeid et al., 2010; Patton et al., 2011). Using data collected by 12 sonic anemometers in two parallel horizontal arrays, Porté-Agel et al. (2001a) found that the $Pr_{SGS}{}^{-1}c_s{}^2$ is strongly stability-dependent and decreases with increasing stability. With the same dataset, Porté-Agel et al. (2001b) further found that Pr_{SGS} is scale-dependent and increases with decreasing z/Δ especially at small z/Δ. Kleissl et al. (2003) analyzed the HATS experimental data and found large variability associated with Pr_{SGS}, which seems to depend weakly on stability and increase with decreasing distance from the ground. Bou-Zeid et al. (2010) combined experimental data collected from the Snow Horizontal Array Turbulence Study (SnoHATS) field campaign (February–April 2006) over the ÒPlaine-MorteÓ glacier in the Swiss Alps and the Lake-Atmosphere Turbulent Exchange (LATEX) field campaign (August–October 2006) over Lake Geneva (Bou-Zeid et al., 2008; Vercauteren et al., 2008) and provided a complete picture of the behavior of Pr_{SGS} across a wide range of stabilities. It was found that Pr_{SGS} decreases as the atmosphere becomes more unstable and increases as the atmosphere become stable with an neutral value of about 0.4 (see Fig. 8).

With the development of dynamic subgrid-scale turbulence models (Germano et al., 1991; Meneveau et al., 1996; Porté-Agel et al., 2000; Bou-Zeid et al., 2005), the Pr_{SGS} can be dynamically computed based on the resolved velocity and temperature fields without invoking any prescribed value or parameterization (Porté-Agel, 2004; Basu and Porté-Agel, 2006; Stoll and Porté-Agel, 2006, 2008). Porté-Agel (2004) proposed a scale-dependent dynamic model for scalar transport and found that the scale-dependence of Pr_{SGS} becomes stronger near the ground, which is consistent with field experimental data (Porté-Agel et al., 2001b). Stoll and Porté-Agel (2006) applied scale-dependent dynamic models to neutral homogeneous and heterogeneous ABLs, while Stoll and Porté-Agel (2008) and Stoll and Porté-Agel (2009) applied them to stable homogeneous and heterogeneous ABLs, respectively. In particular, Stoll and Porté-Agel (2008) presented the averaged values and the probability density functions of Pr_{SGS} (without being lumped with c_s). It is found that the horizontally- and time-averaged Pr_{SGS} is fairly constant throughout the stable ABL (about 0.6) except near the surface where the Pr_{SGS} seems to increase as z decreases. At the boundary layer top, Pr_{SGS} increases as the R_g increases to values larger than unity. The Pr_{SGS} from dynamic models is found to depend strongly on the averaging scheme and also vary with the grid resolution (see also Basu and Porté-Agel (2006)). While these dynamic models can be used to avoid parameterizations of Pr_{SGS} (and to study the behavior of Pr_{SGS}), they are nonetheless computationally expensive. In many cases these dynamic models are only used to compute the Smagorinsky coefficient

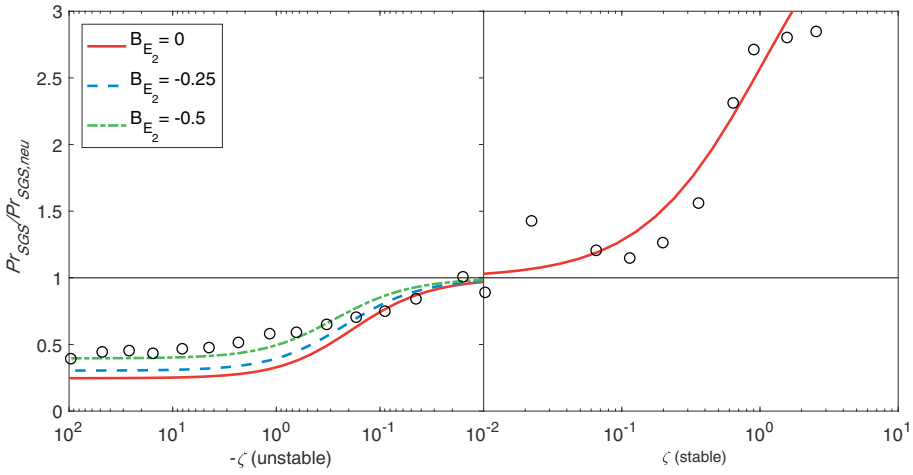

Fig. 8. Comparison between modeled (lines) and measured (circles) Pr_{SGS} (normalized by its neutral value $Pr_{SGS,\ neu} = 0.47$) as a function of the stability parameter ζ. Observational data are taken from field experiments over a lake (Bou-Zeid et al., 2008) and a glacier (Bou-Zeid et al., 2010). Each circle here is the median value of measured Pr_{SGS} over a small range of ζ. This figure is adapted from Li (2016).

while the Pr_{SGS} remains to be parameterized (Kleissl et al., 2006). As such, a simple parameterization for Pr_{SGS} is still desirable even when dynamic models are available.

8.3. The cospectral budget (CSB) model

Li (2016) extended the CSB model presented in Section 7 to studying Pr_{SGS}, particularly its dependence on stability and the filter scale. Instead of integrating the cospectra of momentum and heat fluxes from $k = 0$ to $k = \infty$ as in Section 7, one only needs to integrate the cospectra from the cut-off wavenumber ($k = k_\Delta$) to $k = \infty$ to obtain the subgrid-scale momentum and heat fluxes. Further assuming that the inertial subrange scaling applies for $k > k_\Delta$, which requires that the Ozmidov scale is larger than Δ under stable conditions (Bou-Zeid et al., 2010; Katul et al., 2014; Li et al., 2016b), the SGS momentum and heat fluxes can be evaluated:

$$\tau_{13} = \int_{k_\Delta}^{\infty} F_{uw}(k)dk = \frac{D_2}{(D_1 - 7/3)(4/3)} C_o \varepsilon^{2/3} k_\Delta^{-4/3} + \frac{E_1}{D_1 - 1} k_\Delta^{-D_1+1}, \tag{83}$$

$$h_3 = \int_{k_\Delta}^{\infty} F_{w\theta}(k)dk = \frac{D_4}{(D_3 - 7/3)(4/3)} C_o \varepsilon^{2/3} k_\Delta^{-4/3} Q + \frac{E_2}{D_3 - 1} k_\Delta^{-D_3+1}, \tag{84}$$

where D_1, D_2, D_3, D_4, Q are identical to those presented in Section 7 for the Reynolds-averaged momentum and heat fluxes but with the gradients of the resolved flow variables replacing the gradients of the mean flow variables; E_1 and E_2 are again integration constants.

Interestingly, when $E_1 = E_2 = 0$, which yields a '-7/3' scaling for F_{uw} and $F_{w\theta}$ in the inertial subrange, the Pr_{SGS} from the CSB model has the same stability-dependence as the Pr_t for RANS modeling, namely,

$$Pr_{SGS} = Pr_{SGS,neu} Q^{-1} \tag{85}$$

where Q is also identical to that presented in Section 7. Under such conditions, the filter scale appears to have no influence on the subgrid-scale Pr_t.

When the inertial subrange of $F_{w\theta}$ is 'contaminated' by some anomalous scaling (Bos et al., 2004, 2005; Bos and Bertoglio, 2007), implying that $E_2 \neq 0$, one obtains

$$Pr_{SGS} = Pr_{SGS,neu}(Q + A_s)^{-1}, \tag{86}$$

where

$$A_s = \frac{4}{3} \frac{(A_T/A_{TT} - 2/3)}{(A_T/A_{TT} + 2/3)} k_\Delta^{-\frac{A_T}{A_{TT}} + \frac{2}{3}} \frac{E_2/\Gamma}{D_4 C_{ww}/\Gamma} \tag{87}$$

It is clear that the Pr_{SGS} is now also dependent on the filter scale Δ through the flux-transfer process, which gives rise to E_2. For convenience, the impact of E_2 on $F_{w\theta}$ is assumed to be proportional to the buoyancy term, (i.e., $E_2 = A_{E_2} D_5 C_{TT}$). Substituting the expression for E_2 results in

$$Pr_{SGS} = Pr_{SGS,neu} \left(1 - (1 + B_{E_2}) \frac{1}{1 - C_{IT}} \frac{C_T}{C_o} \frac{\zeta}{\phi_m - \zeta}\right)^{-1}, \tag{88}$$

where $B_{E_2} = \frac{4}{3} \frac{(A_T/A_{TT} - 2/3)}{(A_T/A_{TT} + 2/3)} A_{E_2} k_\Delta^{-\frac{A_T}{A_{TT}} + \frac{2}{3}}$. When $B_{E_2} = 0$, Eq. (88) recovers Eq. (85).

Fig. 8 shows the modeled $Pr_{SGS}/Pr_{SGS,\ neu}$ using Eq. (88) with prescribed values of B_{E_2}. It is clear that the model captures the general trend of SGS Prandtl number reported in recent field experiments (Bou-Zeid et al., 2008, 2010). The model with $B_{E_2} = 0$ captures the trend under stable conditions while $B_{E_2} = -0.5$ better captures the trend under unstable conditions, suggesting that the flux-transfer term, which gives rise to B_{E_2}, is more significant under unstable conditions.

Fig. 9 compares the variations of Pr_{SGS} with respect to the filter scale (Δ) under three unstable regimes to field experimental data taken from Vercauteren et al. (2008). As can be seen, the SGS Prandtl number increases as z/Δ decreases (especially at very low z/Δ values), which is also consistent with other experimental studies (Porté-Agel et al., 2001b) and dynamic model results (Basu and Porté-Agel, 2006; Stoll and Porté-Agel, 2008).

These results suggest that the CSB model can be extended to the subgrid-scale and captures the observed dynamics of Pr_{SGS} reasonably well. The Pr_{SGS} from the CSB model is stability- and scale-dependent. The stability-dependence of Pr_{SGS} is quite similar to that of Pr_t in RANS modeling and the scale-dependence is stronger as the ratio of z/Δ becomes smaller.

9. Concluding remarks and future research priorities

This paper reviews recent advances in our understanding of the turbulent Prandtl number in the ABL, especially in the logarithmic region of the ABL (i.e., the ASL or inertial sublayer) where numerous experimental studies have been conducted. Unlike in engineering flows where the fluid- and Reynolds (or turbulent Peclet) number-dependences of Pr_t are of particular importance, the stability-dependence of Pr_t is the principal concern for atmospheric flows.

For unstable ABLs, researchers discovered the active role of temperature as early as 1940s (Ertel, 1942; Priestley and Swinbank, 1947), which was later confirmed by field experiments including the famous Kansas experiment. Recent work has focused on linking the behavior of Pr_t in unstable ABLs to changes in the turbulence phenomenology. Observations and phenomenological models suggest that the 'scale-resonance' between turbulent eddies and the temperature field enhances

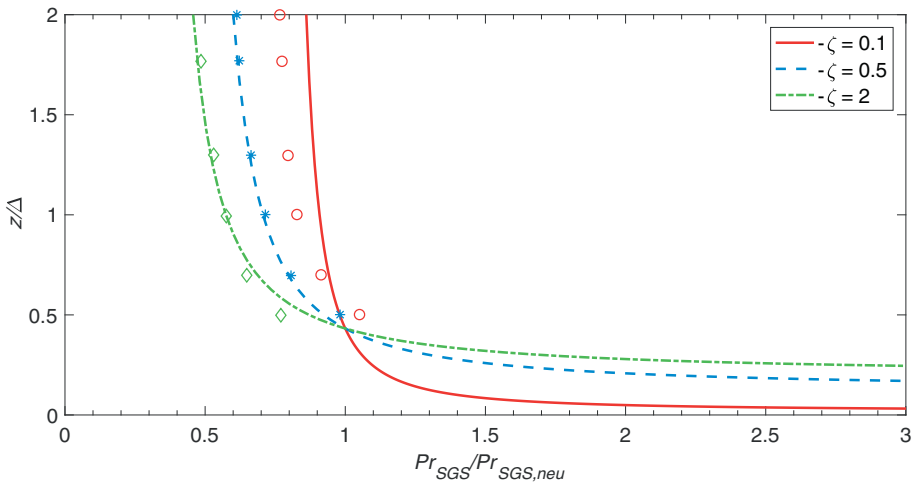

Fig. 9. Comparison between modeled (lines) and measured (markers) Pr_{SGS} (normalized by its neutral value $Pr_{SGS,\ neu} = 0.47$) as a function of z/Δ for three stability regimes. Unlike Fig. 8 only requiring one input parameter (B_{E2}), the model here needs two input parameters (A_{E_2} and A_T/A_{TT}), whose values are −2.7 and 1.08. The observational data collected over a lake surface (Vercauteren et al., 2008) are averaged over three stability regimes ($0 < -\zeta < 0.1$, $0.1 < -\zeta < 1$, $1 < -\zeta$) and thus three predictions with different stability parameters are shown. This figure is adapted from Li (2016).

turbulent transport of heat compared to turbulent transport of momentum, which is responsible for the reduction of Pr_t with increasing instability.

Under stable conditions, using field experimental data to study the stability-dependence of Pr_t (i.e., $Pr_t - \zeta$ and $Pr_t - R_g$ relations) suffers from the issue of 'self-correlation'. Nonetheless, our understanding of Pr_t has greatly benefited from new developments of second-order turbulence closure schemes (e.g., the EFB model) as well as spectral schemes (e.g., the QNSE model). These schemes recover the asymptotic behaviors of Pr_t under near-neutral and very stable conditions, and agree well with observational data and DNS results. One common finding from these new schemes is that turbulent transport is not limited by the critical gradient Richardson number under stable conditions. Instead, the critical gradient Richardson number (and also the maximum flux Richardson number) should be interpreted as the threshold beyond which Monin-Obukhov Similarity Theory (MOST) no longer applies and coincidentally the inertial subrange in the Richardson-Kolmogorov energy cascade dies out.

A unifying framework for Pr_t based on cospectral budgets (CSB) has been developed, which links the macroscopic flow properties (e.g., Pr_t) to the microscale energy distributions governed by the Kolmogorov scaling in the inertial subrange. The CSB model captures the behaviors of Pr_t under both unstable and stable conditions with essentially only two phenomenological constants, and provides a way to unravel the influence of different eddy structures (e.g., the large eddies producing the '-1' scaling) on Pr_t. This model is further applied to investigating the stability- and scale- dependences of the subgrid-scale Prandtl number (Pr_{SGS}), a critical parameter for LES modeling. While the stability-dependence of Pr_{SGS} stems from the buoyancy effect in the resolved flow (similar to the stability-dependence of Pr_t arising from the buoyancy effect in the mean flow), the flux transfer among different turbulent scales is shown to be responsible for the scale-dependence of Pr_{SGS}, especially at small z/Δ where z is the distance from the ground and Δ is the LES filter scale.

The linkages between the macroscopic flow properties and the microscale energy distributions offered by the CSB model shed novel insights on the failure of similarity theories and dimensional considerations in very stable ASL flows (Mahrt, 2014). The collapse of the spectral shapes and the degeneration of the Kolmogorov scaling as the stability increases over a threshold value, as shown by recent field experiments (Grachev et al., 2013), is presumed to be responsible for the this failure. When $R_g > R_{gc}$ or $R_f > R_{f_m}$, experimental data indicate that the shapes of spectra (and cospectra) actually change with changing stability (Li et al., 2015a). This suggests that a unique eddy-energy distribution does not exist, which further implies that the universal character of stability correction functions or Pr_t ceases to exist.

Together with these advances are some long-standing challenges that remain to be addressed, as well as new questions motivated by the recent investigations. In the following, some future research directions and priorities are suggested, which are by no means exhaustive and are only meant to generate discussions.

9.1. The asymptotic behavior of Pr_t as the ABL becomes convective

Despite the unanimous agreement among field experiments on the decrease of Pr_t as instability increases, the asymptotic behavior of Pr_t as the ABL approaches convective conditions (i.e., similar to Rayleigh-Bénard convection) has not been well established (Kader and Yaglom, 1990). Although Pr_t is not well defined under convective conditions, the asymptotic behavior of Pr_t as the ABL approaches the free-convective limit remains important to be understood. The Businger-Dyer relations suggest that Pr_t approaches zero under convective conditions (Fig. 3), implying a zero momentum flux. However, recent studies pointed out the failure of Businger-Dyer relations in capturing the well-known '-1/3' power law scaling (Priestley and Swinbank, 1947; Kaimal et al., 1976) under convective conditions (Wilson, 2001), which arises from the insignificant role of friction velocity in the dimensional analysis when the ABL becomes convective (Wyngaard, 2010). Interestingly, new formulations for ϕ_m and ϕ_h that follow the '-1/3' power law as $-\zeta \to \infty$ yield a non-zero Pr_t under convective conditions (Wilson, 2001), which seems to be also the case for the phenomenological model and the CSB model shown in Fig. 3. These conflicting results suggest that the asymptotic behavior of Pr_t as the ABL becomes convective needs to be further investigated.

9.2. Turbulent momentum and heat transfer in strongly stable ABLs

Quantifying the behavior of Pr_t in strongly stable ABLs also remains a challenge given the previously mentioned issue of 'self-correlation' (Grachev et al., 2007) and the complexities of strongly stable ABLs (Mahrt, 2014). Nearly all theoretical models for Pr_t discussed in this paper explicitly or implicitly invoke the assumption of local equilibrium in the TKE and temperature variance budgets, that is, the shear production and the buoyant production/destruction balance the dissipation. The evidence in the literature thus far seems to be in support of such approximations for unstable conditions when data are conditioned for stationarity and planar homogeneity in the absence of subsidence (Hsieh and Katul, 1997; Charuchittipan and Wilson, 2009; Salesky et al., 2013) but the picture is far less clear for stable conditions (Salesky et al., 2013), especially for very stable conditions (Li et al., 2016b).

As a result of our poor understanding of turbulent transport in

strongly stable ABLs, there are many ad-hoc treatments in stable boundary layer parameterizations in weather and climate models. For example, most numerical models tend to increase the eddy viscosity and diffusivity under strongly stable conditions in order to avoid 'run-away cooling' (Holtslag et al., 2013; Sandu et al., 2013). In addition, certain schemes still have a critical gradient Richardson number (like the MY model) and when the gradient Richardson number exceeds this critical value, the model switches to some other parameterizations (see e.g., Lindvall et al. (2017)). Model results are unfortunately quite sensitive to these treatments (Derbyshire, 1999; Fernando and Weil, 2010; Holtslag et al., 2013). This calls for more investigations of momentum and heat transfer in strongly stable ABLs, which has important implications for improving weather forecasts and climate predictions.

9.3. The dissimilarity between heat and mass transfer

As mentioned in the introduction, nearly all atmospheric models assume that other scalars, such as water vapor, CO_2, methane, and ozone, are transported similarly as heat. This assumption can break down as temperature is an active scalar that alters the air flow through creating buoyancy, while the other scalars have very small or negligible effects on the air flow (note here radiative and microphysical processes are not considered). The dissimilarity between turbulent transport of heat and moisture from the perspective of flux-gradient relation has been studied (Warhaft, 1976; Brost, 1979; Lee et al., 2004; Katul et al., 2016). Scalar dissimilarity is also investigated in terms of flux-variance relation (Katul and Hsieh, 1999; Williams et al., 2007; Detto et al., 2008), transport efficiency (Moriwaki and Kanda, 2006; Wang et al., 2014), structure function (Li et al., 2012a; Maronga, 2014; Maronga et al., 2014), and covariance and correlation (Sempreviva and Højstrup, 1998; De Bruin et al., 1999; Asanuma et al., 2007; Katul et al., 2008; Moene and Schüttemeyer, 2008). However, no operational formulations have been proposed to account for scalar dissimilarity. In addition, how chemical reactions induce dissimilarity between transport of heat and reactive scalars and the scale-dependence of such dissimilarity (i.e., chemical reactions often occur at very small scales while turbulent diffusivity is a quantity describing the transport capacity of turbulent motions of all scales) remain to be investigated.

9.4. The vertical profile of Pr_t

While the Pr_t in the ASL has been widely studied, its vertical variation throughout the ABL is less known. Based on laboratory data, Rotta (1964) proposed the expression $Pr_t = 0.9 - 0.4(z/\delta)^2$, where δ is the boundary layer height (Reynolds, 1975). However, using wind-tunnel measurements, Koeltzsch (2000) found that the turbulent Schmidt number increases with increasing height when $z/\delta < 0.3$ and decreases with increasing height when $z/\delta > 0.3$ in a neutrally stratified turbulent boundary layer. Kastner-Klein and Fedorovich (2002) found no direct evidence of height-dependence of the turbulent Schmidt number in a wind-tunnel model of neutral ABL. These inconsistent results even in controlled lab experiments under neutrally stratified conditions clearly demonstrate the need to investigate the vertical profile of Pr_t.

As a result of this lack of understanding, current stable ABL parameterizations often assume that the same $Pr_t - R_g$ relation applies everywhere in the atmosphere (Tastula et al., 2015a) or some ad-hoc vertical variations in the $Pr_t - R_g$ relation (Sandu et al., 2013). These assumptions have no theoretical justification and have not been evaluated experimentally. It is pointed out that the profile of Pr_t is only meaningful under neutral or stable conditions. Under unstable (especially convective) conditions, the applicability of flux-gradient relations breaks down in the mixed layer where non-local transport is important (Holtslag and Moeng, 1991; Wyngaard and Weil, 1991; Holtslag and Boville, 1993; Zilitinkevich et al., 1999; van Dop and Verver, 2001).

9.5. The importance of Pr_t in weather and climate models

Studies examining the role of Pr_t in weather and climate models were surprisingly sparse. Earlier generations of atmospheric models often assume that Pr_t equals to its neutral value under all stable conditions motivated by the Businger-Dyer relations. Lee et al. (2006) found that allowing Pr_t to increase with stability, as Fig. 6 suggests, alleviates the problem of overestimation of heat diffusion and reduces surface temperature biases. Tastula et al. (2015a) demonstrated that the choice of $Pr_{t,\,neu}$ in the ASL parameterization affects the vertical profiles of temperature and humidity throughout the entire boundary layer. Interestingly, they found that the choice of $Pr_{t,\,neu}$ is sometimes even more important than the functional form that determines the stability dependence of ϕ_h. A global study showed that reducing the value of $Pr_{t,\,neu}$ from unity to 0.8 warms and moistens low-latitude boundary layers and reduces some long-standing biases in the stratocumulus regions, the Southern Ocean and the equatorial cold tongue (Pithan et al., 2015). On the other hand, a study using single-column model found insignificant changes in the vertical profiles of mean potential temperature and heat flux when the Pr_t is reduced from 1 to 0.85 (Huang et al., 2013). These findings suggest that our understanding of how Pr_t affects the flow and temperature (and other scalar) fields, what feedbacks Pr_t generates, and under what conditions such feedbacks are important remains limited. More studies are needed to systematically investigate the sensitivity of simulation results to the parameterization of Pr_t in weather and climate models.

Acknowledgments

This work is funded by US Army Research Office (Grant W911NF-18-1-0360). I would like to thank Professor Gabriel Katul at Duke University, Professor Elie Bou-Zeid at Princeton University, and Dr. Sergej Zilitinkevich at Finnish Meteorological Institute for their inspiration and collaboration on this research topic.

References

Abe, H., Kawamura, H., Matsuo, Y., 2004. Surface heat-flux fluctuations in a turbulent channel flow up to $Re_\tau = 1020$ with $Pr = 0.025$ and 0.71. Int. J. Heat Fluid Flow 25, 404–419.
Adrian, R.J., 2007. Hairpin vortex organization in wall turbulence. Phys. Fluids 19, 041301.
Aliabadi, A.A., Staebler, R.M., Liu, M., Herber, A., 2016. Characterization and parametrization of Reynolds stress and turbulent heat flux in the stably-stratified lower arctic troposphere using aircraft measurements. Bound. Layer Meteorol. 161, 99–126.
Anderson, P.S., 2009. Measurement of Prandtl number as a function of Richardson number avoiding self-correlation. Bound. Layer Meteorol. 131, 345–362.
Andreas, E.L., 2002. Parameterizing scalar transfer over snow and ice: a review. J. Hydrometeorol. 3, 417–432.
Antonia, R., Chambers, A., Friehe, C., Van Atta, C., 1979. Temperature ramps in the atmospheric surface layer. J. Atmos. Sci 36, 99–108.
Asanuma, J., Tamagawa, I., Ishikawa, H., Ma, Y., Hayashi, T., Qi, Y., Wang, J., 2007. Spectral similarity between scalars at very low frequencies in the unstable atmospheric surface layer over the tibetan plateau. Boundary-layer meteorology 122, 85–103.
Baas, P., de Roode, S.R., Lenderink, G., 2008. The scaling behaviour of a turbulent kinetic energy closure model for stably stratified conditions. Bound. Layer Meteorol. 127, 17–36.
Bange, J., Roth, R., 1999. Helicopter-borne flux measurements in the nocturnal boundary layer over land–a case study. Bound. Layer Meteorol. 92, 295–325.
Basu, S., Porté-Agel, F., 2006. Large-eddy simulation of stably stratified atmospheric boundary layer turbulence: A scale-dependent dynamic modeling approach. J. Atmos. Sci 63, 2074–2091.
Bos, W., Bertoglio, J., 2007. Inertial range scaling of scalar flux spectra in uniformly sheared turbulence. Phys. Fluids 19, 025104–025111.
Bos, W., Touil, H., Shao, L., Bertogli, J., 2004. On the behavior of the velocity-scalar cross correlation spectrum in the inertial range. Phys. Fluids 16, 3818–3823.
Bos, W., Touil, H., Bertoglio, J., 2005. Reynolds number dependency of the scalar flux spectrum in isotropic turbulence with a uniform scalar gradient. Phys. Fluids 17 (125), 108–126.
Bou-Zeid, E., Meneveau, C., Parlange, M., 2005. A scale-dependent lagrangian dynamic model for large eddy simulation of complex turbulent flows. Phys. Fluids 17, 025105.
Bou-Zeid, E., Vercauteren, N., Parlange, M., Meneveau, C., 2008. Scale dependence of subgrid-scale model coefficients: An a priori study. Phys. Fluids 20.

Bou-Zeid, E., Higgins, C., Huwald, H., Parlange, M., Meneveau, C., 2010. Field study of the dynamics and modeling of subgrid scale turbulence in a stable atmospheric surface layer over a glacier. J. Fluid Mech. 665, 480–515.
Brost, R., 1979. Some comments on the turbulent exchange coefficients for sensible heat and water vapor under advective conditions. J. Appl. Meteorol. 18, 378–380.
Brown, A., Derbyshire, S., Mason, P., 1994. Large-eddy simulation of stable atmospheric boundary layers with a revised stochastic subgrid model. Q. J. R. Meterol. Soc. 120, 1485–1512.
Brunet, Y., Collineau, S., Shaw, R.H., Maitani, T., Qiu, J., Hipps, L., et al., 1992. On coherent structures in turbulence above and within agricultural plant canopies. Agric. For. Meteorol. 61, 55–68.
Businger, J.A., 1988. A note on the Businger-Dyer profiles. Bound. Layer Meteorol. 42, 145–151.
Businger, J.A., Yaglom, A.M., 1971. Introduction to Obukhov's paper on 'Turbulence in an atmosphere with a non-uniform temperature'. Bound. Layer Meteorol. 2, 3–6.
Businger, J.A., Wyngaard, J.C., Izumi, Y., Bradley, E.F., 1971. Flux-profile relationships in the atmospheric surface layer. J. Atmos. Sci. 28, 181–191.
Cantwell, B.J., 1981. Organized motion in turbulent flow. Annu. Rev. Fluid Mech. 13, 457–515.
Canuto, V.M., Cheng, Y., Howard, A., Isau, I., 2008. Stably stratified flows: A model with no Ri(cr). J. Atmos. Sci. 65, 2437–2447. https://doi.org/10.1175/2007JAS2470.1.
Carper, M.A., Porté-Agel, F., 2004. The role of coherent structures in subfilter-scale dissipation of turbulence measured in the atmospheric surface layer. J. Turbul. 5, 32.
Cava, D., Katul, G., 2012. On the scaling laws of the velocity-scalar cospectra in the canopy sublayer above tall forests. Bound. Layer Meteorol. 145, 351–367.
Charuchittipan, D., Wilson, J., 2009. Turbulent kinetic energy dissipation in the surface layer. Bound. Layer Meteorol. 132, 193–204.
Chauhan, K., Hutchins, N., Monty, J., Marusic, I., 2013. Structure inclination angles in the convective atmospheric surface layer. Bound. Layer Meteorol. 1–10.
Chung, D., Matheou, G., 2012. Direct numerical simulation of stationary homogeneous stratified sheared turbulence. J. Fluid Mech. 696, 434–467.
Corrsin, S., 1961. The reactant concentration spectrum in turbulent mixing with a first-order reaction. J. Fluid Mech. 11, 407–416. https://doi.org/10.1017/S0022112061000615.
De Bruin, H., Van Den Hurk, B., Kroon, L., 1999. On the temperature-humidity correlation and similarity. Bound. Layer Meteorol. 93, 453–468.
de Roode, S.R., Jonker, H.J., van de Wiel, B.J., Vertregt, V., Perrin, V., 2017. A diagnosis of excessive mixing in Smagorinsky subfilter-scale turbulent kinetic energy models. J. Atmos. Sci 74, 1495–1511.
Deardorff, J., 1973. The use of subgrid transport equations in a three-dimensional model of atmospheric turbulence. J. Fluids Eng 95, 429–438.
Deardorff, J., 1980. Stratocumulus-capped mixed layers derived from a three-dimensional model. Bound. Layer Meteorol. 18, 495–527.
Derbyshire, S., 1999. Stable boundary-layer modeling: established approaches and beyond. Bound. Layer Meteorol. 90, 423–446.
Detto, M., Katul, G., Mancini, M., Montaldo, N., Albertson, J., 2008. Surface heterogeneity and its signature in higher-order scalar similarity relationships. Agric. For. Meteorol. 148, 902–916.
Dyer, A., 1974. A review of flux-profile relationships. Bound. Layer Meteorol. 7, 363–372.
Elliott, Z.A., Venayagamoorthy, S.K., 2011. Evaluation of turbulent Prandtl (Schmidt) number parameterizations for stably stratified environmental flows. Dyn. Atmos. Oceans 51, 137–150.
Ertel, H., 1942. Ein neuer hydrodynamischer wirbelsatz. Meteorol. Z. 59, 277–281.
Fernando, H., Weil, J., 2010. Whither the stable boundary layer? A shift in the research agenda. Bull. Amer. Meteorol. Soc. 91, 1475–1484.
Ferrero, E., Quan, L., Massone, D., 2011. Turbulence in the stable boundary layer at higher Richardson numbers. Bound. Layer Meteorol. 139, 225–240.
Foken, T., 2006. 50 years of the Monin-Obukhov similarity theory. Bound. Layer Meteorol. 119, 431–447.
Frisch, U., 1995. Turbulence: the Legacy of AN Kolmogorov. Cambridge University Press.
Galperin, B., Sukoriansky, S., 2010. Geophysical flows with anisotropic turbulence and dispersive waves: flows with stable stratification. Ocean Dyn. 60, 1319–1337.
Galperin, B., Sukoriansky, S., Anderson, P.S., 2007. On the critical Richardson number in stably stratified turbulence. Atmosph. Sci. Lett. 65–69.
Germano, M., Piomelli, U., Moin, P., Cabot, W.H., 1991. A dynamic subgrid-scale eddy viscosity model. Phys. Fluids 3, 1760–1765.
Gibbs, J.A., Fedorovich, E., 2016. Sensitivity of turbulence statistics in the lower portion of a numerically simulated stable boundary layer to parameters of the deardorff subgrid turbulence model. Q. J. R. Meteorol. Soc. 142, 2205–2213.
Gioia, G., Guttenberg, N., Goldenfeld, N., Chakraborty, P., 2010. Spectral theory of the turbulent mean-velocity profile. Phys. Rev. Lett. 105.
Grachev, A., Andreas, E., Fairall, C., Guest, P., Persson, P.G., 2007. On the turbulent Prandtl number in the stable atmospheric boundary layer. Bound. Layer Meteorol. 329–341.
Grachev, A., Andreas, E., Fairall, C., Guest, P., Persson, P.G., 2013. The critical Richardson number and limits of applicability of local similarity theory in the stable boundary layer. Bound. Layer Meteorol. 51–82.
Grisogono, B., 2010. Generalizing 'z-less' mixing length for stable boundary layers. Q. J. R. Meteorol. Soc. 136, 213–221.
Guala, M., Metzger, M., McKeon, B., 2010. Intermittency in the atmospheric surface layer: Unresolved or slowly varying? Physica D 239, 1251–1257.
Gualtieri, C., Angeloudis, A., Bombardelli, F., Jha, S., Stoesser, T., 2017. On the values for the turbulent Schmidt number in environmental flows. Fluids 2, 17.
Högström, U., 1988. Non-dimensional wind and temperature profiles in the atmospheric surface layer: A re-evaluation. Bound. Layer Meteorol. 1–2, 55–78.
Högström, U., 1996. Review of some basic characteristics of the atmospheric surface layer. Bound. Layer Meteorol. 78, 215–246.
Holtslag, A., Boville, B., 1993. Local versus nonlocal boundary-layer diffusion in a global climate model. J. Climate 6, 1825–1842.
Holtslag, A., Moeng, C.H., 1991. Eddy diffusivity and countergradient transport in the convective atmospheric boundary layer. J. Atmos. Sci 48, 1690–1698.
Holtslag, A.A.M., et al., 2013. Stable atmospheric boundary layers and diurnal cycles: Challenges for weather and climate models. Bull. Amer. Meteorol. Soc. 94, 1691–1706.
Hommema, S.E., Adrian, R.J., 2003. Packet structure of surface eddies in the atmospheric boundary layer. Bound. Layer Meteorol. 106, 147–170.
Horst, T., Kleissl, J., Lenschow, D., Meneveau, C., Moeng, C.H., Parlange, M., Sullivan, P., Weil, J., 2004. Hats: Field observations to obtain spatially filtered turbulence fields from crosswind arrays of sonic anemometers in the atmospheric surface layer. J. Atmos. Sci. 61, 1566–1581.
Howard, L.N., 1961. Note on a paper of John W. Miles. J. Fluid Mech. 10, 509–512.
Howell, J., Sun, J., 1999. Surface-layer fluxes in stable conditions. Bound. Layer Meteorol. 90, 495–520.
Hsieh, C.I., Katul, G.G., 1997. Dissipation methods, Taylor's hypothesis, and stability correction functions in the atmospheric surface layer. J. Geophys. Res.: Atmos. 102 (16), 391–16,405.
Huang, J., Bou-Zeid, E., Golaz, J.C., 2013. Turbulence and vertical fluxes in the stable atmospheric boundary layer. Part ii: A novel mixing-length model. J. Atmos. Sci. 70, 1528–1542.
Hutchins, N., Chauhan, K., Marusic, I., Monty, J., Klewicki, J., 2012. Towards reconciling the large-scale structure of turbulent boundary layers in the atmosphere and laboratory. Bound. Layer Meteorol. 145, 273–306.
Ishihara, T., Yoshida, K., Kaneda, Y., 2002. Anisotropic velocity correlation spectrum at small scales in a homogeneous turbulent shear flow. Phys. Rev. Lett. 88. https://doi.org/10.1103/PhysRevLett.88.154501.
Kader, B., Yaglom, A., 1990. Mean fields and fluctuation moments in unstably stratified turbulent boundary layers. J. Fluid Mech. 212, 637–662. https://doi.org/10.1017/S0022112090002129.
Kader, B., Yaglom, A., 1991. Spectra and correlation functions of surface layer atmospheric turbulence in unstable thermal stratification. In: Metais, O., Lesieur, M. (Eds.), Turbulence and Coherent Structures. Kluwer Academic Publishers, USA, pp. 450–467.
Kaimal, J.C., 1973. Turbulence spectra, length scales and structure parameters in the stable surface layer. Bound. Layer Meteorol. 4, 289–309.
Kaimal, J., Finnigan, J., 1994. Atmospheric Boundary Layer Flows: Their Structure and Measurement. Oxford University Press, New York.
Kaimal, J.C., Izumi, Y., Wyngaard, J.C., Cote, R., 1972. Spectral characteristics of surface-layer turbulence. Q. J. R. Meteorol. Soc. 98, 563–589.
Kaimal, J., Wyngaard, J., Haugen, D., Coté, O., Izumi, Y., Caughey, S., Readings, C., 1976. Turbulence structure in the convective boundary layer. J. Atmos. Sci 33, 2152–2169.
Kajishima, T., Taira, K., 2017. Computational Fluid Dynamics. Springer.
Kang, H.S., Meneveau, C., 2002. Universality of large eddy simulation model parameters across a turbulent wake behind a heated cylinder. J. Turbul. 3, 26.
Kasagi, N., Tomita, Y., Kuroda, A., 1992. Direct numerical simulation of passive scalar field in a turbulent channel flow. J. Heat Transfer 114, 598–606.
Kastner-Klein, P., Fedorovich, E., 2002. Diffusion from a line source deployed in a homogeneous roughness layer: interpretation of wind-tunnel measurements by means of simple mathematical models. Atmos. Environ. 36, 3709–3718.
Katul, G., Chu, C., 1998. A theoretical and experimental investigation of energy-containing scales in the dynamic sublayer of boundary-layer flows. Bound. Layer Meteorol. 86, 279–312.
Katul, G.G., Hsieh, C.I., 1999. A note on the flux-variance similarity relationships for heat and water vapor in the unstable atmospheric surface layer. Bound. Layer Meteorol. 90, 327–338.
Katul, G.G., Manes, C., 2014. Cospectral budget of turbulence explains the bulk properties of smooth pipe flow. Phys. Rev. E 90, 063008. https://doi.org/10.1103/PhysRevE.90.063008.
Katul, G., Chu, C., Parlange, M., Albertson, J., Ortenburger, T., 1995. Low-wavenumber spectral characteristics of velocity and temperature in the atmospheric surface layer. J. Geophys. Res. 100, 14,243–14,255.
Katul, G.G., Sempreviva, A.M., Cava, D., 2008. The temperature–humidity covariance in the marine surface layer: a one-dimensional analytical model. Boundary-Layer Meteorol. 126, 263–278.
Katul, G., Konings, A., Porporato, A., 2011. Mean velocity profile in a sheared and thermally stratified atmospheric boundary layer. Phys. Rev. Lett. 107.
Katul, G., Li, D., Chamecki, M., Bou-Zeid, E., 2013a. Mean scalar concentration profile in a sheared and thermally stratified atmospheric surface layer. Phys. Rev. E. 87.
Katul, G., Porporato, A., Manes, C., Meneveau, C., 2013b. *Co*-spectrum and mean velocity in turbulent boundary layers. Phys. Fluids 25, 091702.
Katul, G., Porporato, A., Shah, S., Bou-Zeid, E., 2014. Two phenomenological constants explain similarity laws in stably stratified turbulence. Phys. Rev. E. 89.
Katul, G.G., Li, D., Liu, H., Assouline, S., 2016. Deviations from unity of the ratio of the turbulent Schmidt to Prandtl numbers in stratified atmospheric flows over water surfaces. Phys. Rev. Fluids 1, 034401.
Kawamura, H., Ohsaka, K., Abe, H., Yamamoto, K., 1998. DNS of turbulent heat transfer in channel flow with low to medium-high Prandtl number fluid. Int. J. Heat Fluid Flow 19, 482–491.
Kawamura, H., Abe, H., Matsuo, Y., 1999. DNS of turbulent heat transfer in channel flow with respect to Reynolds and Prandtl number effects. Int. J. Heat Fluid Flow 20, 196–207.
Kays, W., 1994. Turbulent Prandtl number-Where are we? J. Heat Transf. 116, 284–295.
Kim, J., Mahrt, L., 1992. Simple formulation of turbulent mixing in the stable free

atmosphere and nocturnal boundary layer. Tellus A 44, 381–394.
Kitamura, Y., Hori, A., Yagi, T., 2013. Flux Richardson number and turbulent Prandtl number in a developing stable boundary layer. J. Meteorl. Soc. Japan. 91, 655–666.
Kleissl, J., Meneveau, C., Parlange, M.B., 2003. On the magnitude and variability of subgrid-scale eddy-diffusion coefficients in the atmospheric surface layer. J. Atmos. Sci. 60, 2372–2388.
Kleissl, J., Kumar, V., Meneveau, C., Parlange, M.B., 2006. Numerical study of dynamic Smagorinsky models in large-eddy simulation of the atmospheric boundary layer: Validation in stable and unstable conditions. Water Resour. Res 42.
Koeltzsch, K., 2000. The height dependence of the turbulent Schmidt number within the boundary layer. Atmos. Environ. 34, 1147–1151.
Kolmogorov, A., 1941. The local structure of turbulence in imcompressible viscous fluid for very large reynolds numbers. Dokl. Akad. Nauk. SSSR 30, 299–303.
Kondo, J., Kanechika, O., Yasuda, N., 1978. Heat and momentum transfers under strong stability in the atmospheric surface layer. J. Atmos. Sci. 35, 1012–1021.
Kong, H., Choi, H., Lee, J.S., 2000. Direct numerical simulation of turbulent thermal boundary layers. Phys. Fluids 12, 2555–2568.
Kurbatskii, A., Kurbatskaya, L., 2010. On the turbulent Prandtl number in a stably stratified atmospheric boundary layer. Izv. Atmos. Ocean. Phys. 46, 169–177.
Kurbatskiy, A., Kurbatskaya, L., 2014. Eddy mixing in planetary boundary layer and free atmosphere. In: 20th International Symposium on Atmospheric and Ocean Optics: Atmospheric Physics, International Society for Optics and Photonics, pp. 92920R.
Launder, B., Reece, G., Rodi, W., 1975. Progress in the development of a Reynolds-stress turbulence closure. J. Fluid Mech. 68, 537–566.
Lee, X., Yu, Q., Sun, X., Liu, J., Min, Q., Liu, Y., Zhang, X., 2004. Micrometeorological fluxes under the influence of regional and local advection: a revisit. Agric. For. Meteorol. 122, 111–124.
Lee, S.M., Giori, W., Princevac, M., Fernando, H., 2006. Implementation of a stable PBL turbulence parameterization for the mesoscale model MM5: nocturnal flow in complex terrain. Bound. Layer Meteorol. 119, 109–134.
Li, D., 2016. Revisiting the subgrid-scale Prandtl number for large-eddy simulation. J. Fluid Mech. 802, R2. https://doi.org/10.1017/jfm.2016.472.
Li, D., Bou-Zeid, E., 2011. Coherent structures and the dissimilarity of turbulent transport of momentum and scalars in the unstable atmospheric surface layer. Bound. Layer Meteorol. 140, 243–262.
Li, D., Katul, G.G., 2017. On the linkage between the $k^{-5/3}$ spectral and $k^{-7/3}$ cospectral scaling in high-Reynolds number turbulent boundary layers. Phys. Fluids 29, 065108.
Li, D., Bou-Zeid, E., de Bruin, H., 2012a. Monin-Obukhov similarity functions for the structure parameters of temperature and humidity. Boundary-Layer Meteorol. 145, 45–67.
Li, D., Katul, G., Bou-Zeid, E., 2012b. Mean velocity and temperature profiles in a sheared diabatic turbulent boundary layer. Phys. Fluids 24.
Li, D., Katul, G., Bou-Zeid, E., 2015a. Turbulent energy spectra and cospectra of momentum and heat fluxes in the stable atmospheric surface layer. Bound. Layer Meteorol. 157, 1–21.
Li, D., Katul, G.G., Zilitinkevich, S.S., 2015b. Revisiting the turbulent Prandtl number in an idealized atmospheric surface layer. J. Atm. Sci. 72, 2394–2410.
Li, D., Katul, G.G., Zilitinkevich, S.S., 2016a. Closure schemes for stably stratified atmospheric flows without turbulence cutoff. J. Atmos. Sci. 73, 4817–4832.
Li, D., Salesky, S., Banerjee, T., 2016b. Connections between the Ozmidov scale and mean velocity profile in stably stratified atmospheric surface layers. J. Fluid Mech. 797, 11. https://doi.org/10.1017/jfm.2016.311.
Lilly, D., 1967. The representation of small scale turbulence in numerical simulation experiments. In: IBM Scientific Computing Symposium on Environmental Sciences, pp. 195–210.
Lindvall, J., Svensson, G., Caballero, R., 2017. The impact of changes in parameterizations of surface drag and vertical diffusion on the large-scale circulation in the Community Atmosphere Model (CAM5). Clim. Dyn. 48, 3741–3758.
Liu, Y., Mamtimin, A., Huo, W., Yang, X., Liu, X., Yang, F., He, Q., 2016. Nondimensional wind and temperature profiles in the atmospheric surface layer over the hinterland of the Taklimakan Desert in China. Adv. Meteorol. 2016.
Liu, H.Y., Bo, T.L., Liang, Y.R., 2017. The variation of large-scale structure inclination angles in high Reynolds number atmospheric surface layers. Phys. Fluids 29, 035104.
Louis, J.F., Tiedtke, M., Geleyn, J.F., 1982. A short history of the operational PBL-parameterization at ECMWF. In: ECMWF Workshop Planetary Boundary Layer Parameterization, pp. 59–79.
Lumley, J., 1964. The spectrum of nearly inertial turbulence in a stably stratified fluid. J. Atmos. Sci. 21, 99–102.
Lumley, J.L., Panofsky, H.A., 1964. The Structure of Atmospheric Turbulence. John Wiley.
Mahrt, L., 1998. Stratified atmospheric boundary layers and breakdown of models. Theor. Computat. Fluid Dyn. 11, 263–279.
Mahrt, L., 2014. Stably stratified atmospheric boundary layers. Annu. Rev. Fluid Mech. 46, 23–45.
Maronga, B., 2014. Monin–obukhov similarity functions for the structure parameters of temperature and humidity in the unstable surface layer: Results from high-resolution large-eddy simulations. J. Atmos. Sci. 71, 716–733.
Maronga, B., Hartogensis, O.K., Raasch, S., Beyrich, F., 2014. The effect of surface heterogeneity on the structure parameters of temperature and specific humidity: a large-eddy simulation case study for the LITFASS-2003 experiment. Bound. Layer Meteorol. 153, 441–470.
Marusic, I., McKeon, B.J., Monkewitz, P.A., Nagib, H.M., Smits, A.J., Sreenivasan, K.R., 2010. Wall-bounded turbulent flows at high Reynolds numbers: Recent advances and key issues. Phys. Fluids 22.
Mason, P., 1989. Large-eddy simulation of the convective atmospheric boundary layer. J. Atmos. Sci. 46, 1492–1516.
Mason, P., Brown, A., 1999. On subgrid models and filter operations in large eddy simulations. J. Atmos. Sci. 56, 2101–2114.
McColl, K.A., van Heerwaarden, C.C., Katul, G.G., Gentine, P., Entekhabi, D., 2017. Role of large eddies in the breakdown of the Reynolds analogy in an idealized mildly unstable atmospheric surface layer. Q. J. R. Meteorol. Soc. 143, 2182–2197.
Mellor, G.L., 1973. Analytic prediction of the properties of stratified planetary surface layers. J. Atmos. Sci. 30, 1061–1069.
Mellor, G.L., Yamada, T., 1974. A hierarchy of turbulence closure models for planetary boundary layers. J. Atm. Sci. 31, 1791–1806.
Mellor, G.L., Yamada, T., 1982. Development of a turbulence closure model for geophysical fluid problems. Rev. Geophys. 20, 851–875.
Meneveau, C., Lund, T.S., Cabot, W.H., 1996. A Lagrangian dynamic subgrid-scale model of turbulence. J. Fluid Mech. 319, 353–385.
Miles, J.W., 1961. On the stability of heterogeneous shear flows. J. Fluid Mech. 10, 496–508.
Moene, A.F., Schüttemeyer, D., 2008. The effect of surface heterogeneity on the temperature–humidity correlation and the relative transport efficiency. Bound. Layer Meteorol. 129, 99–113.
Moeng, C.H., Wyngaard, J.C., 1986. An analysis of closures for pressure-scalar covariances in the convective boundary layer. J. Atmos. Sci 43, 2499–2513.
Moeng, C., Wyngaard, J., 1988. Spectral analysis of large-eddy simulations of the convective boundary layer. J. Atmos. Sci. 45, 3573–3587.
Monin, A., Obukhov, A., 1954. Basic laws of turbulent mixing in the ground layer of the atmosphere. Akad. Nauk. SSSR. Geofiz. Inst. Trudy 151, 163–187.
Monin, A., Yaglom, A., 1971. Statistical Fluid Mechanics. 1 MIT Press, Cambridge, MA.
Monti, P., Fernando, H., Princevac, M., Chan, W., Kowalewski, T., Pardyjak, E., 2002. Observations of flow and turbulence in the nocturnal boundary layer over a slope. J. Atmos. Sci. 59, 2513–2534.
Moriwaki, R., Kanda, M., 2006. Local and global similarity in turbulent transfer of heat, water vapor, and CO2 in the dynamic convective sublayer over a suburban area. Bound. Layer Meteorol. 120, 163–179.
Nakanish, M., 2001. Improvement of the Mellor-Yamada turbulence closure model based on large-eddy simulation data. Bound. Layer Meteorol. 99, 349–378.
Obukhov, A., 1946. Turbulence in thermally inhomogeneous atmosphere. Trudy Inta Teoret. Geofiz. Akad. Nauk S.S.S.R. 95–115.
Ohya, Y., 2001. Wind-tunnel study of atmospheric stable boundary layers over a rough surface. Bound. Layer Meteorol. 98, 57–82.
Panchev, S., 1971. Random Functions and Turbulence. Pergamon Press, New York.
Pardyjak, E., Monti, P., Fernando, H., 2002. Flux Richardson number measurements in stable atmospheric shear flows. J. Fluid Mech. 459, 307–316.
Patton, E.G., Horst, T.W., Sullivan, P.P., Lenschow, D.H., Oncley, S.P., Brown, W.O., Burns, S.P., Guenther, A.B., Held, A., Karl, T., et al., 2011. The canopy horizontal array turbulence study. Bull. Amer. Meteorol. Soc. 92, 593–611.
Patton, E.G., Sullivan, P.P., Shaw, R.H., Finnigan, J.J., Weil, J.C., 2016. Atmospheric stability influences on coupled boundary layer and canopy turbulence. J. Atmos. Sci. 73, 1621–1647.
Pithan, F., Angevine, W., Mauritsen, T., 2015. Improving a global model from the boundary layer: Total turbulent energy and the neutral limit Prandtl number. J. Adv. Model. Earth Syst. 7, 791–805.
Pope, S., 2000. Turbulent Flows. Cambridge University Press, Cambridge, UK.
Porté-Agel, F., 2004. A scale-dependent dynamic model for scalar transport in large-eddy simulations of the atmospheric boundary layer. Bound. Layer Meteorol. 112, 81–105.
Porté-Agel, F., Meneveau, C., Parlange, M., 2000. A scale-dependent dynamic model for large-eddy simulation: application to a neutral atmospheric boundary layer. J. Fluid Mech. 415, 261–284.
Porté-Agel, F., Pahlow, M., Meneveau, C., Parlange, M.B., 2001a. Atmospheric stability effect on subgrid-scale physics for large-eddy simulation. Adv. Water Resour. 24, 1085–1102.
Porté-Agel, F., Parlange, M., Meneveau, C., Eichinger, W., 2001b. A priori field study of the subgrid-scale heat fluxes and dissipation in the atmospheric surface layer. J. Atmos. Sci. 58, 2673–2698.
Priestley, C., Swinbank, W., 1947. Vertical transport of heat by turbulence in the atmosphere. Proc. R. Soc. Lond. A 189, 543–561.
Redjem-Saad, L., Ould-Rouiss, M., Lauriat, G., 2007. Direct numerical simulation of turbulent heat transfer in pipe flows: Effect of Prandtl number. Int. J. Heat Fluid Flow 28, 847–861.
Reynolds, A., 1975. The prediction of turbulent Prandtl and Schmidt numbers. Int. J. Heat Mass Transfer 18, 1055–1069.
Robinson, S.K., 1991. Coherent motions in the turbulent boundary layer. Annu. Rev. Fluid Mech. 23, 601–639.
Rodrigo, J.S., Anderson, P.S., 2013. Investigation of the stable atmospheric boundary layer at Halley Antarctica. Bound. Layer Meteorol. 148, 517–539.
Rohr, J.J., Itsweire, E.C., Helland, K.N., Atta, C.W.V., 1988. Growth and decay of turbulence in a stably stratified shear flow. J. Fluid Mech. 195, 77–111.
Rohsenow, W.M., Hartnett, J.P., Cho, Y.I., et al., 1998. Handbook of Heat Transfer. Vol. 3 McGraw-Hill, New York.
Rotta, J., 1951. Statistical theory of nonhomogeneous turbulence. Z. Physik 131.
Rotta, J., 1964. Temperaturverteilungen in der turbulenten grenzschicht an der ebenen platte. Int. J. Heat Mass Transfer 7, 215–228.
Saddoughi, S., Veeravalli, S., 1994. Local isotropy in turbulent boundary layers at high Reynolds number flow. J. Fluid Mech. 268, 333–372.
Salesky, S.T., Katul, G.G., Chamecki, M., 2013. Buoyancy effects on the integral lengthscales and mean velocity profile in atmospheric surface layer flows. Phys. Fluids 25.
Salesky, S.T., Chamecki, M., Bou-Zeid, E., 2017. On the nature of the transition between roll and cellular organization in the convective boundary layer. Bound. Layer

Meteorol. 163, 41–68.
Sandu, I., Beljaars, A., Bechtold, P., Mauritsen, T., Balsamo, G., 2013. Why is it so difficult to represent stably stratified conditions in numerical weather prediction (NWP) models? J. Adv. Model. Earth Syst. 5, 117–133.
Schmidt, H., Schumann, U., 1989. Coherent structure of the convective boundary layer derived from large-eddy simulations. J. Fluid Mech. 200, 511–562.
Schumann, U., 1991. Subgrid length-scales for large-eddy simulation of stratified turbulence. Theor. Comp. Fluid Dyn. 2, 279–290.
Schumann, U., Gerz, T., 1995. Turbulent mixing in stably stratified shear flows. J. Appl. Meteorol. 34, 33–48.
Schumann, U., Grötzbach, G., Kleiser, L., 1980. Direct numerical simulation of turbulence. In: Prediction Methods for Turbulent Flows, pp. 123–258.
Sempreviva, A.M., Højstrup, J., 1998. Transport of temperature and humidity variance and covariance in the marine surface layer. Bound. Layer Meteorol. 87, 233–253.
Shah, S., Bou-Zeid, E., 2014a. Very-large-scale motions in the atmospheric boundary layer educed by snapshot proper orthogonal decomposition. Bound. Layer Meteorol. 153, 355–387.
Shah, S.K., Bou-Zeid, E., 2014b. Direct numerical simulations of turbulent ekman layers with increasing static stability: modifications to the bulk structure and second-order statistics. J. Fluid Mech. 760, 494–539.
Shih, L., Koseff, J., Ferziger, J., Rehmann, C., 2000. Scaling and parameterisation of stratified homogeneous turbulent shear flow. J. Fluid Mech. 412, 1–20.
Smits, A.J., McKeon, B.J., Marusic, I., 2011. High-Reynolds number wall turbulence. Annu. Rev. Fluid Mech. 43, 353–375.
Song, X., Zhang, H., Chen, J., Park, S.U., 2010. Flux–gradient relationships in the atmospheric surface layer over the Gobi Desert in China. Bound. Layer Meteorol. 134, 487–498.
Sorbjan, Z., Grachev, A.A., 2010. An evaluation of the flux–gradient relationship in the stable boundary layer. Bound. Layer Meteorol. 135, 385–405.
Sreenivasan, K.R., 1995. On the universality of the Kolmogorov constant. Phys. Fluids 7, 2778–2784.
Sreenivasan, K.R., 1996. The passive scalar spectrum and the Obukhov-Corrsin constant. Phys. Fluids 8, 189–196.
Stensrud, D., 2007. Parameterization Schemes: Keys to Understanding Numerical Weather Prediction Models. Cambridge University Press, Cambridge.
Stoll, R., Porté-Agel, F., 2006. Dynamic subgrid-scale models for momentum and scalar fluxes in large-eddy simulations of neutrally stratified atmospheric boundary layers over heterogeneous terrain. Water Resour. Res. 42.
Stoll, R., Porté-Agel, F., 2008. Large-eddy simulation of the stable atmospheric boundary layer using dynamic models with different averaging schemes. Bound. Layer Meteorol. 126, 1–28.
Stoll, R., Porté-Agel, F., 2009. Surface heterogeneity effects on regional-scale fluxes in stable boundary layers: Surface temperature transitions. J. Atm. Sci. 66, 412–431.
Strang, E., Fernando, H., 2001. Vertical mixing and transports through a stratified shear layer. J. Phys. Oceanogr. 31, 2026–2048.
Stretch, D., Rottman, J., Venayagamoorthy, S., Nomura, K.K., Rehmann, C.R., 2010. Mixing efficiency in decaying stably stratified turbulence. Dyn. Atmos. Oceans 49, 25–36.
Stull, R., 1988. An Introduction to Boundary Layer Meteorology. Kluwer Academic Publishers, Dordrecht.
Sukoriansky, S., Galperin, B., Perov, V., 2005a. Application of a new spectral theory of stably stratified turbulence to the atmospheric boundary layer over sea ice. Bound. Layer Meteorol. 117, 231–257.
Sukoriansky, S., Galperin, B., Staroselsky, I., 2005b. A quasinormal scale elimination model of turbulent flows with stable stratification. Phys. Fluids 17, 085107.
Sukoriansky, S., Galperin, B., Perov, V., 2006. A quasi-normal scale elimination model of turbulence and its application to stably stratified flows. Nonlin. Processes Geophys. 13, 9–22.
Sun, J., Nappo, C.J., Mahrt, L., Belušic, D., Grisogono, B., Stauffer, D.R., Pulido, M., Staquet, C., Jiang, Q., Pouquet, A., et al., 2015. Review of wave-turbulence interactions in the stable atmospheric boundary layer. Rev. Geophys. 53, 956–993.
Tastula, E.M., Galperin, B., Dudhia, J., LeMone, M.A., Sukoriansky, S., Vihma, T., 2015a. Methodical assessment of the differences between the QNSE and MYJ PBL schemes for stable conditions. Q. J. R. Meteorol. Soc. 141, 2077–2089.
Tastula, E.M., Galperin, B., Sukoriansky, S., Luhar, A., Anderson, P., 2015b. The importance of surface layer parameterization in modeling of stable atmospheric boundary layers. Atmos. Sci. Lett. 16, 83–88.
Tastula, E.M., LeMone, M.A., Dudhia, J., Galperin, B., 2016. The impact of the QNSE-EDMF scheme and its modifications on boundary layer parameterization in WRF: modeling of CASES-97. Q. J. R. Meteorol. Soc. 142, 1182–1195.
Taylor, G.I., 1915. Eddy motion in the atmosphere. Phil. Trans. R. Soc. Lond. A 215, 1–26.
Taylor, G., 1938. The spectrum of turbulence. Proc. R. Soc. Lond., A 132, 476–490.
Tennekes, H., Lumley, J., 1972. A First Course in Turbulence. MIT Press, Cambridge, MA.
Tominaga, Y., Stathopoulos, T., 2013. CFD simulation of near-field pollutant dispersion in the urban environment: A review of current modeling techniques. Atmos. Environ. 79, 716–730.
Townsend, A., 1976. The Structure of Turbulent Shear Flow. Cambridge University Press, Cambridge, MA.
Turner, J.S., 1979. Buoyancy Effects in Fluids. Cambridge University Press, Cambridge, MA.
van Dop, H., Verver, G., 2001. Countergradient transport revisited. J. Atmos. Sci 58, 2240–2247.
Vasil'ev, O., Voropaeva, O., Kurbatskii, A., 2011. Turbulent mixing in stably stratified flows of the environment: The current state of the problem. Izv. Atmos. Ocean. Phys. 47, 265–280.
Venayagamoorthy, S., Stretch, D., 2010. On the turbulent Prandtl number in homogeneous stably stratified turbulence. J. Fluid Mech. 644, 359–369.
Vercauteren, N., Bou-Zeid, E., Parlange, M.B., Lemmin, U., Huwald, H., Selker, J., Meneveau, C., 2008. Subgrid-scale dynamics for water vapor, heat, and momentum over a lake. Bound. Layer Meteorol. 128, 205–228.
Wang, L., Li, D., Gao, Z., Sun, T., Guo, X., Bou-Zeid, E., 2014. Turbulent transport of momentum and scalars above an urban canopy. Bound. Layer Meteorol. 150, 485–511.
Warhaft, Z., 1976. Heat and moisture flux in the stratified boundary layer. Q. J. R. Meteorol. Soc. 102, 703–707.
Webster, C., 1964. An experimental study of turbulence in a density-stratified shear flow. Dyn. Atmos. Oceans 19, 221–245.
Williams, C.A., Scanlon, T.M., Albertson, J.D., 2007. Influence of surface heterogeneity on scalar dissimilarity in the roughness sublayer. Bound. Layer Meteorol. 122, 149.
Wilson, D.K., 2001. An alternative function for the wind and temperature gradients in unstable surface layers. Bound. Layer Meteorol. 99, 151–158.
Wyngaard, J.C., 1985. Structure of the planetary boundary layer and implications for its modeling. J. Climate Appl. Meteor. 24, 1131–1142.
Wyngaard, J.C., 2010. Turbulence in the Atmosphere. Cambridge University Press.
Wyngaard, J., Cote, O., 1972. *Co*-spectral similarity theory in the atmospheric surface layer. Q. J. R. Meteorol. Soc. 98, 590–603.
Wyngaard, J.C., Weil, J.C., 1991. Transport asymmetry in skewed turbulence. Phys. Fluids 3, 155–162.
Yakhot, V., Orszag, S.A., Yakhot, A., 1987. Heat transfer in turbulent fluids - I. pipe flow. Int. J. Heat Mass Transfer 30, 15–22.
Yamada, T., 1975. The critical Richardson number and the ratio of the eddy transport coefficients obtained from a turbulence closure model. J. Atmos. Sci 32, 926–933.
Yeung, P., Zhou, Y., 1997. Universality of the Kolmogorov constant in numerical simulations of turbulence. Phys. Rev. E. 56, 1746.
Zhang, Y., Liu, H., Foken, T., Williams, Q.L., Mauder, M., Thomas, C., 2011. Coherent structures and flux contribution over an inhomogeneously irrigated cotton field. Theor. Appl. Climatol. 103, 119–131.
Zilitinkevich, S., Calanca, P., 2000. An extended similarity theory for the stably stratified atmospheric surface layer. Q. J. R. Meteorol. Soc. 126, 1913–1923.
Zilitinkevich, S., Gryanik, V.M., Lykossov, V., Mironov, D., 1999. Third-order transport and nonlocal turbulence closures for convective boundary layers. J. Atmos. Sci 56, 3463–3477.
Zilitinkevich, S., Elperin, T., Kleeorin, N., Rogachevskii, I., 2007. Energy- and flux-budget (EFB) turbulence closure model for stably stratified flows. Part I: steady-state, homogeneous regimes. Bound. Layer Meteorol. 125, 167–192.
Zilitinkevich, S., Elperin, T., Kleeorin, N., Rogachevskii, I., Esau, I., Mauritsen, T., Miles, M., 2008. Turbulence energetics in stably stratified geophysical flows: Strong and weak mixing regimes. Q. J. R. Meteorol. Soc. 134, 793–799.
Zilitinkevich, S., Elperin, T., Kleeorin, N., L'vov, V., Rogachevskii, I., 2009. Energy-and flux-budget turbulence closure model for stably stratified flows. Part II: the role of internal gravity waves. Bound. Layer Meteorol. 133, 139–164.
Zilitinkevich, S., Elperin, T., Kleeorin, N., Rogachevskii, I., Esau, I., 2013. A hierarchy of energy- and flux-budget (EFB) turbulence closure models for stably-stratified geophysical flows. Bound. Layer Meteorol. 146, 341–373.
Zúñiga-Zamalloa, C., Ng, H.C.H., Chakraborty, P., Gioia, G., 2014. Spectral analogues of the law of the wall, the defect law and the log law. J. Fluid Mech. 757, 498–513.